Revision 2

Word Count: 9419

Mineralogical and geochemical facets of the massive deposition of stibnite-metastibnite at a seafloor hydrothermal field (Wakamiko Crater, Kagoshima Bay, Ryukyu Volcanic Arc)

VESSELIN DEKOV[1,*], YUKAKO FURUMA[1], BLEUENN GUÉGUEN[2,3], LUKAS KLOSE[4], KAZUTAKA YASUKAWA[5,6], MOTOAKI MORITA[7], DAN ASAEL[8], TOSHIRO YAMANAKA[1], LUCA BINDI[9], ANDREA KOSCHINSKY[4], BERNHARD PRACEJUS[10], YASUHIRO KATO[5,6,11,12]

[1]Department of Ocean Sciences, Tokyo University of Marine Science and Technology, 4-5-7 Konan, Minato-ku, Tokyo 108-8477, Japan
[2]CNRS, Univ Brest, UMR 6538 Laboratoire Géosciences Océan, F-29280 Plouzané, France
[3]CNRS, Univ Brest, UMS 3113, F-29280 Plouzané, France
[4]Department of Physics and Earth Sciences, Constructor University Bremen gGmbH, Campus Ring 1, 28759 Bremen, Germany
[5]Frontier Research Center for Energy and Resources, School of Engineering, The University of Tokyo, Bunkyo-ku, Tokyo 113-8656, Japan
[6]Department of Systems Innovation, School of Engineering, The University of Tokyo, 7-3-1 Hongo, Bunkyo-ku, Tokyo 113-8656, Japan
[7]Department of Marine Electronics and Mechanical Engineering, Tokyo University of Marine Science and Technology, 2-1-6 Etchujima, Koto-ku, Tokyo 135-8533, Japan
[8]Department of Geology and Geophysics, Yale University, New Haven, CT 06520, USA
[9]Dipartimento di Scienze della Terra, Università degli Studi di Firenze, Via Giorgio La Pira 4, I-50121, Firenze, Italy

[*] E-mail: vdekov0@kaiyodai.ac.jp. Orcid 0000-0002-2369-0337

[10]Department of Earth Sciences, Sultan Qaboos University, PO Box 36, 123 Al-Khoud, Muscat, Sultanate of Oman

[11]Ocean Resources Research Center for Next Generation, Chiba Institute of Technology, 2-17-1 Tsudanuma, Narashino, Chiba 275-0016, Japan

[12]Submarine Resources Research Center, Research Institute for Marine Resources Utilization, Japan Agency for Marine-Earth Science and Technology (JAMSTEC), 2-15 Natsushima-cho, Yokosuka, Kanagawa 237-0061, Japan

ABSTRACT

Stibnite precipitates in the form of massive boulders at two active hydrothermal mounds in the submarine Wakamiko Crater (Ryukyu Volcanic Arc) as opposed to commonly observed accessory stibnite in the seafloor hydrothermal deposits. The stibnite dimorph, metastibnite, found here for the first time on the seafloor, appears to always form whenever stibnite is precipitated under submarine hydrothermal conditions. Our study shows that hydrothermal conditions of low temperatures (<50 °C) and low values of *pH* (<6) are favorable for the precipitation of stibnite on the seafloor. The stibnite probably does not precipitate at the measured vent fluid temperatures (i.e., 177.6 – 187.0 °C) along the chimney conduits, but rather at temperatures <50 °C and at slightly reduced to slightly oxic conditions (*Eh* = -0.5 to +0.5 V) within the chimney walls and hydrothermal mounds. Metastibnite deposition appears to be the result of rapid quenching of hot hydrothermal fluid when mixed with cold seawater and rapid precipitation at the interface between stibnite and vent fluid. The low concentrations (usually below detection limits) of the trace elements (Cd, Co, Cr, Cu, Li, Mn, Mo, Ni, P, Pb, Sr, V, Zn) in the stibnite deposits from Wakamiko Crater are likely a result of decreased metal-transporting capacity of the precipitating vent fluid due to its low chlorinity. Low-chlorinity venting implies sub-seafloor boiling and phase separation of the hydrothermal fluid. Sluggish hydrothermal fluid/seawater mixing within the walls of the chimneys and mounds favors the reduction of sulfate dissolved in the hydrothermal fluids and results in a heavy S isotope composition of the sulfate in the vent fluids. Sulfate reduction and disproportionation of magmatic SO_2, both leading to heavy S isotope composition of sulfate in the vent fluids, seem to be common processes in volcanic arc/back-arc submarine hydrothermal settings.

Keywords: Hydrothermal, metastibnite, stibnite, sulfate reduction, Wakamiko Crater

INTRODUCTION

Stibnite (Sb_2S_3) is a rare and accessory mineral in the seafloor hydrothermal deposits. It has been found in hydrothermal deposits located along submarine volcanic arc (Nedachi et al. 1991; Dekov and Savelli 2004; Yamanaka et al. 2013), back-arc (Halbach et al. 1993; Nakashima et al. 1995; Okamoto et al. 2002; Ooki et al. 2012; Dekov et al. 2022) and fore-arc (Petersen et al. 2002) tectonic settings. Stibnite appears to be scarce in hydrothermal deposits at mid-ocean ridge (MOR) setting (Firstova et al. 2016). It was also observed to precipitate in artificially induced, seafloor hydrothermal chimneys in a back-arc rift (Iheya-North vent field, Okinawa Trough; Nozaki et al. 2016). Therefore, occurrence of this apparently rare sulfide as boulders in hydrothermal mounds in a submarine volcanic crater (Wakamiko Crater, Kagoshima Bay, Ryukyu Volcanic Arc; Yamanaka et al. 2013) attracts particular scientific interest. This occurrence implies uncommon conditions for hydrothermal precipitation (volatile element concentrations, *T*, *P*, *pH*, *Eh*), which have persisted over a prolonged time interval.

Data on metastibnite (Sb_2S_3), an X-ray semi-amorphous dimorph of stibnite, is rare in the literature (Becker 1888; Hunt 1888; Brookins 1970; Mozgova et al. 1977; Olivier-Fourcade et al. 1983). Similarly, we are not aware of any occurrence of metastibnite on the seafloor.

Given the limited knowledge on the stibnite and metastibnite precipitation at seafloor hydrothermal conditions, we studied the stibnite-bearing deposits and venting hydrothermal fluids of Wakamiko Crater (Ryukyu Volcanic Arc, Japan). To evaluate whether metastibnite always forms whenever stibnite precipitates under seafloor hydrothermal conditions, we investigated metastibnite occurrence in six stibnite-bearing samples recovered from two other seafloor hydrothermal fields, namely, Daisan-Kume Knoll (Ryukyu Arc) and Daiyon-Yonaguni Knoll (Okinawa Trough).

GEOLOGICAL SETTING

Wakamiko Crater is located in the eastern part of the Kagoshima Bay, Kyushu Island, and represents the northeastern-most extension of the Ryukyu Arc (Fig. 1 **a**) (Yamanaka et al. 2013).

Kagoshima Bay encompasses the submerged Aira and Ata calderas, and the active Wakamiko and Sakurajima volcanoes (not shown in Fig. 1 **b**). The Wakamiko Crater (Fig. 1 **b**) is interpreted to have formed during the Ito eruption ~25000 yr B.P. (Aramaki 1984). The seafloor of the crater (~200 m depth) is covered by ~80 m thick sediment (Hayasaka 1987). Fumarolic activity (Ôki and Hayasaka 1978) and anomalies of relatively high concentrations of volatile elements such as Sb, As, and Hg in the sediments in and around the crater, indicate the existence of active magma chamber beneath the crater (Sakamoto 1985). Three sites discharging focused and relatively hot fluids, and three other sites emanating diffuse (shimmering) hydrothermal fluids, have been reported for the Wakamiko Crater (Yamanaka et al. 2013). The Hairy Cone (T_{max} = 198.6 °C; Figs 1 **b**, 2 **a**) and White Cone (T_{max} = 187 °C; Figs 1 **b**, 2 **b**) chimney-mound sites are composed of a few-meters-thick-mounds of blackish, boulder-sized rubble of sulfides crowned by ~2 m tall whitish chimneys, whereas the Daifukuyama site (T_{max} = 111 °C) is a mound (Yamanaka et al. 2013).

Daisan-Kume Knoll is a felsic submarine volcano located to the west of Kumejima Island, Ryukyu Arc (Fig. 1 **a**). This volcanic edifice has two calderas: one to the north and another to the south (Minami and Ohara 2017). Surveys conducted by a remotely operated vehicle (ROV) in the southern caldera (Harigane 2015) found evidence for hydrothermal activity (i.e., a chimney field, sulfide deposits, altered rocks, and venting of shimmering fluids), which showed that Daisan-Kume Knoll is indeed a hydrothermally active volcano.

Daiyon-Yonaguni Knoll is a seamount located in the southernmost part of the Okinawa Trough (Matsumoto et al. 2001) (Fig. 1 **a**). An active hydrothermal field of the same name is located in an elongated depression covered by thick, muddy sediment adjacent to this seamount (Gena et al. 2005). Four major hydrothermal chimney–mound complexes were observed to discharge both black and clear, relatively hot fluids (Konno et al. 2006; Suzuki et al. 2008; Fujiwara et al. 2015). Diffuse, low-temperature venting was observed in the southern part of the hydrothermal field (Suzuki et al. 2008).

SAMPLES AND METHODS OF INVESTIGATION

Samples

In our attempt to characterize the mineralogy and geochemistry of massive stibnite precipitated under seafloor hydrothermal conditions, we studied three stibnite-containing samples collected during the August 2008 R/V

Natsushima cruise NT08-17 from two hydrothermal mounds in the Wakamiko Crater (Table 1; Fig. 3). The samples recovered from the Hairy Cone and White Cone hydrothermal sites were black to grayish-black, fragile chunks of mound structures (Fig. 3 **a**, **b**, **c**). Sub-samples (small chunks, ~3 g) from each sample were ground to fine powders in an agate mortar for mineralogical and geochemical analyses. Polished thin sections were prepared from each sample for optical microscopy and electron microprobe studies.

In addition, six samples of seafloor hydrothermal deposits (finely powdered) recovered from the Daiyon-Yonaguni Knoll, Okinawa Trough (5) and Daisan-Kume Knoll, Ryukyu Arc (1) (Table 1), that contained stibnite (Dekov et al. 2022; and Harigane 2015, respectively) were investigated for the presence of metastibnite only.

Two vent fluid samples recovered during the May 2007 R/V *Natsushima* cruise NT07-09 were collected from the White Cone vent using multi-cylinder polycarbonate sample bottles with a rotary switching valve system with an all-titanium sample inlet and attached temperature probe (Table 2). The vent fluid samples were filtered (0.45 μm membrane filters), acidified immediately after recovery, and stored in high density polyethylene (HDPE) bottles for further onshore analyses.

Methods of investigation

Details of the methods of investigation of the (1) mineralogy, chemistry and S isotope composition of the hydrothermal deposits, (2) chemistry and S isotope composition of the hydrothermal fluids, and (3) modeling of stability phase diagrams can be found in the Supplementary online material.

RESULTS

Mineralogy of the hydrothermal deposits

XRD investigations (Tables 3, 4; Fig. 4 **a**) show that stibnite is the main mineral in all the Wakamiko Crater samples, consistent with initial macroscopic observations of hand specimens. The calculated unit-cell parameters of this stibnite are reported in Table 5. Stibnite is also present in the Daisan-Kume Knoll (Harigane 2015) and Daiyon-Yonaguni Knoll (Dekov et al. 2022) hydrothermal deposits.

Stibnite in the Wakamiko Crater hydrothermal deposits appears as two forms: long (>100 μm), both thick (~20 μm) and thin (~2 μm) prismatic crystals (Figs 5 **a**, **b**; 6 **b**, **c**), and rosettes of needle-like crystals (Figs 5 **c**-**h**; 6 **a**). In reflected cross-polarized light, stibnite crystal terminations (Fig. 5 **d**), crystal peripheries (Fig. 5 **f**), or entire crystals (Fig. 5 **h**) show red internal reflections. As stibnite never shows such red internal reflections, there are two possible explanations of these optical features. The first is oxidation of stibnite (at crystal terminations, at crystal peripheries, or the entire crystal) to kermesite (Sb_2S_2O), which typically shows red

internal reflections in reflected cross-polarized light. However, there is no evidence from XRD of kermesite in the samples (Table 3). The second possibility is the presence of metastibnite, which also shows red internal reflections in reflected cross-polarized light. Metastibnite has the same mineral chemistry as stibnite (Sb_2S_3), but is X-ray semi-amorphous, usually showing two weak peaks between 56.2 and 56.5 °2θ (Cu K_α radiation), a region where there are not any stibnite peak. XRD analysis of random samples in the range 55.5 - 57.0 °2θ using small steps and slow speed (see Supplementary online material, Mineralogy of hydrothermal deposits) produced XRD patterns with an asymmetric peak between 55.9 and 56.5 °2θ, i.e., slightly displaced towards lower angles than those of metastibnite (Fig. 4 **b**). This strongly suggests that in addition to stibnite, the Wakamiko Crater samples also contain metastibnite. Similar XRD patterns were obtained for the samples from the stibnite-containing hydrothermal deposits from Daisan-Kume Knoll and Daiyon-Yonaguni Knoll (Fig. 4 **c**, **d**). This suggests that all the studied stibnite-containing samples contain metastibnite as well. The shape of this metastibnite peak (i.e., asymmetry, intensity) and its displacement relative to the standard metastibnite peak (Lafuente et al. 2015) are different for different samples (Fig. 4 **b**-**d**).

Sulfur, Sb, and As are homogeneously distributed within both morphological types of Wakamiko Crater stibnite, i.e., prismatic (Fig. 7) and rosettes of needle-like crystals (Fig. 8).

The chemistry of the Wakamiko Crater stibnite is very close to stoichiometry with rare, minor As and Sn contents (Table 6).

Furthermore, a weak, broad (hump-like) peak centered at ~7.5 °2θ appears in the XRD patterns of all the Wakamiko Crater stibnite samples (Fig. 4 **a**). The presence of disordered talc in the Wakamiko Crater hydrothermal deposits was reported in a previous study (Yamanaka et al. 2013). However, the main peak (00*1*) of the disordered talc is at ~9 °2θ. The location of the observed hump-like peak (Fig. 4 **a**) at lower angles than that of the 00*1* peak of the disordered talc might imply the presence of mixed-layer talc-smectites. However, as we have not performed detailed investigations for clay minerals, we can only assume that talc-smectite is present in traces in the samples.

Geochemistry of the Wakamiko Crater hydrothermal deposits

The almost pure stibnite samples from the Wakamiko Crater have high Sb, Mg, Al, Fe and Na contents and low (mostly below the detection limits) Ca, Cd, Co, Cr, Cu, K, Li, Mn, Mo, Ni, P, Pb, Sr, V, Zn contents (Table 7).

Geochemistry of the Wakamiko Crater hydrothermal fluids

The concentrations of Fe, Sb, Mn, Zn, Mo, Ni and V were relatively high, whereas the concentrations of U, Pb, Co, Cd, Y, and Cu were relatively low in the Wakamiko Crater venting fluids (Table 8). REE concentrations were particularly low, being mostly below the detection limits (Table 8). Cerium anomalies (Ce/Ce*), calculated relative to Nd (because the Pr concentrations were below the detection limit), were slightly positive in both vent fluid samples (Table 8; Fig. 9). The Eu anomaly, calculated relative to Nd (as Sm concentrations were below the detection limit) in one vent fluid sample only, was strongly positive (Table 8; Fig. 9). The REE distribution pattern of the analyzed seawater standard (CASS-6) followed that of the North Pacific Deep Water (Alibo and Nozaki 1999) and shows both negative Ce and Eu anomalies (Table 8; Fig. 9).

S isotope composition of the Wakamiko Crater hydrothermal deposits and fluids

Sulfur isotope composition (sulfide S) of the studied Wakamiko Crater hydrothermal deposits ranges from 2.8 to 3.6 ‰ (Table 7). Vent fluids from the White Cone vent (Table 2) have S isotope composition (sulfate S) heavier than that of average modern seawater ($\delta^{34}S_{sulfate}$ = 20.97 ± 0.10 ‰; Paris et al. 2013) (Table 8).

Modeling of stability phase diagrams

Using the chemistry data for the studied vent fluid samples (Table 8), we have produced a number of stability phase diagrams with the GWB. In principle, at the seafloor hydrothermal sites the hydrothermal fluids are discharged in two modes: (1) focused, flow through the chimney orifice, and (2) diffused, percolation through the porous chimney walls and mound structures, and slow cooling (conductive and through mixing with seawater) of the fluid. We modeled stability phase diagrams at the measured venting temperatures (Table 8) with the assumption of focused fluid discharge and stibnite precipitation along the chimney conduit in contact with the venting

This is the peer-reviewed, final accepted version for American Mineralogist, published by the Mineralogical Society of America.
The published version is subject to change. Cite as Authors (Year) Title. American Mineralogist, in press.
DOI: https://doi.org/10.2138/am-2023-9096. http://www.minsocam.org/

fluid. As the studied stibnite comes from the hydrothermal mound boulders, we also modeled stability phase diagrams related to diffuse discharge through the hydrothermal mound. We supposed fluid temperatures lower than that of the venting fluid (Table 8) and decreasing (150 °C, 100 °C, 50 °C and 25 °C) away from a hypothetical conduit of discharge. For simplicity of the modeling and interpretations, we assumed fluid cooling due only to mixing with seawater, but used the chemistry of the fluids venting through the chimney orifice (Table 8). Unfortunately, the "thermo_minteq" database does not contain data for metastibnite and we were not able to model the stability fields of this mineral.

In the modeling, we considered all the possible aqueous Sb species (ions) that were available in the "thermo_minteq" database. Because dissolved H_2S ($H_2S_{(aq)}$) is the main reduced species in the hydrothermal fluids that, upon reaction with metal and metalloid ions forms metal and metalloid sulfides (e.g., Sb_2S_3), we considered the activity of $H_2S_{(aq)}$ as one of the main variables in the modeling. The attempt to model $\log_{10}\mathbf{a}[H_2S_{(aq)}]$-$\log_{10}\mathbf{a}[SbCl_4^+]$ diagram produced an empty plot. The diagram $\log_{10}\mathbf{a}[H_2S_{(aq)}]$-$\log_{10}\mathbf{a}[(NH_4)Sb_2S_4^-]$ showed just $(NH_4)Sb_2S_4^-$ ion throughout the entire temperature range. Diagrams using the $Sb_2S_4^{2-}$ ion ($\log_{10}\mathbf{a}[H_2S_{(aq)}]$-$\log_{10}\mathbf{a}[Sb_2S_4^{2-}]$, Eh-$\log_{10}\mathbf{a}[Sb_2S_4^{2-}]$) were identical to those for $Sb(OH)_{3(aq)}$. The diagrams for both vent fluid samples (687R1 and 687R3) were very similar and therefore, we have shown and discussed the stability phase diagrams $\log_{10}\mathbf{a}[H_2S_{(aq)}]$-$\log_{10}\mathbf{a}[HSb_2S_4^-]$, $\log_{10}\mathbf{a}[H_2S_{(aq)}]$-$\log_{10}\mathbf{a}[Sb(OH)_{3(aq)}]$ and $\log_{10}\mathbf{a}[H_2S_{(aq)}]$-*Eh* for sample 687R1 only (Fig. 10).

DISCUSSION

Precipitation of stibnite and metastibnite under seafloor hydrothermal conditions

The solubility of stibnite and ion speciation of Sb at hydrothermal conditions are largely controlled by temperature and *pH* (Wilson et al. 2007; Brown 2011). The solubility of stibnite decreases by a few orders of magnitude with a drop in temperature of only a few tens of degrees C (within temperature range 200 – 25 °C) and also with a drop in *pH* of 2-3 units (from slightly alkaline to slightly acid) (Brown 2011). Therefore, low-temperature and low *pH* hydrothermal conditions are conducive to stibnite precipitation and will lead to a quantitative removal of Sb from the hydrothermal solution (Wilson et al. 2007; Brown 2011). In such conditions, stibnite

239 was observed to precipitate as long needle-like crystals (Brown 2011). However, when Sb_2S_3
240 precipitates rapidly rather metastibnite forms (Brown 2011).

241 Previous observations (e.g., Wilson et al. 2007; Brown 2011) of stibnite precipitation under
242 hydrothermal conditions suggest that at the relatively low-temperature (177.6-187.0 °C) and *pH*
243 (5.86-5.99) conditions of the White Cone vent (Wakamiko Crater) (Table 2), massive stibnite
244 could precipitate. The crystal habit of the Wakamiko Crater stibnite, i.e., long prismatic crystals
245 and rosettes of needle-like crystals (Figs 5, 6, 8), is also consistent with previous observations for
246 the crystal habit of hydrothermally precipitated stibnite (Brown 2011). Similar rosettes of blade-
247 like barite crystals precipitated at other seafloor hydrothermal sites were interpreted to be
248 indicative of quenching and rapid precipitation from mixing hydrothermal fluid and seawater (de
249 Ronde et al. 2003, 2005, 2011; Berkenbosch et al. 2012).

250 The stability phase diagram modeling shows that at the measured venting temperatures
251 (177.6 °C and 187.0 °C; Table 8), the stibnite is stable at $\log_{10}\mathbf{a}[H_2S_{(aq)}] > -4.5$, $\log_{10}\mathbf{a}[HSb_2S_4^-]$
252 > -4.5 and $\log_{10}\mathbf{a}[Sb(OH)_{3(aq)}] > -4.2$ (Fig. 10 **a**, **e**). With decreasing temperature, the stability
253 field of stibnite enlarges (Fig. 10 **b**, **c**, **d**, **f**, **g**, **h**). However, the $\log_{10}\mathbf{a}[H_2S_{(aq)}]$-*Eh* diagrams show
254 that stibnite starts precipitating below 50 °C (Fig. 10 **k**) and its stability field enlarges with
255 decreasing temperature (Fig. 10 **l**). We can conclude, therefore, that stibnite most probably does
256 not precipitate at the measured venting temperatures in the chimney conduits, but rather at
257 temperatures below 50 °C and at slightly reduced to slightly oxic (*Eh* = -0.5 – +0.5 V) conditions
258 (Fig. 10) within the chimney walls and mounds.

259 The occurrence of metastibnite at crystal terminations and margins of Wakamiko Crater
260 stibnite (Figs 5 **c**-**h**), when combined with previous observations of metastibnite precipitation
261 (Brown 2011), suggest that: (1) metastibnite is not an alteration product after stibnite, (2) it is
262 rather a product of rapid quenching of the hot hydrothermal fluid upon mixing with cold seawater
263 with rapid precipitation at the interface between stibnite and the vent fluid. We suggest that due
264 to rapid precipitation, the Sb_2S_3 cannot form an ordered crystal structure (i.e., stibnite), but rather
265 occurs in a semi-amorphous state (i.e., metastibnite). The occurrence of metastibnite together
266 with stibnite also in the other two stibnite-containing seafloor hydrothermal sites (Daisan-Kume
267 Knoll and Daiyon-Yonaguni Knoll) implies that if stibnite precipitates under seafloor
268 hydrothermal conditions, then metastibnite will always form alongside it. The slight displacement

of the metastibnite peaks towards lower angles in the XRD patterns (Fig. 4 **b-d**) may be due to isomorphic replacement of As for Sb in the metastibnite structure.

Unit-cell parameters of stibnite from Wakamiko Crater (Table 5) are close to those of pure stibnite (Kyono and Kimata 2004). The small deviations could be due to minor replacement of As and Sn for Sb (Table 6).

Geochemistry of the Wakamiko Crater hydrothermal deposits: A result of boiling and phase separation of the hydrothermal fluid

A fundamental feature of the seawater chemistry is that the major ions are present in relatively constant ratios. These constant ratios are not necessarily maintained in the seafloor (seawater-based) hydrothermal fluids because of the gains and losses of elements during sub-seafloor seawater-rock interactions. Chlorine is a conservative element during these interactions. Thus, the element/Cl ratios in the hydrothermal fluids are indicators for gains or losses of elements relative to the starting fluid (seawater). Na/Cl of the Wakamiko Crater end-member hydrothermal fluid (0.83) is slightly lower than that of the ambient seawater (0.86) [Table 1 in Yamanaka et al. (2013)]. This means that the seawater has lost a small fraction of its Na during seawater reaction with the basement rocks, presumably due to albitization (German and Von Damm, 2003): Na for Ca replacement reaction in plagioclase. However, the negligible loss of Na from seawater due to its interaction with the crustal rocks and the maintenance of Na/Cl ratio of the fluid (seawater → end-member hydrothermal fluid) is less important than the net decrease in the concentrations of both Na and Cl in the end-member hydrothermal fluid ([Na] = 232 mM, [Cl] = 279 mM) in respect to the seawater ([Na] = 464 mM, [Cl] = 541 mM) (Yamanaka et al., 2013). The observed decrease in fluid chlorinity (salinity) by about 50 % seems to be most likely a result of sub-seafloor boiling of the fluid and its phase separation in high- and low-chlorinity fluids (Von Damm, 1990). Obviously, the studied vent fluids (Table 8) represent the low-chlorinity fractions of the phase-separated fluids. As chloride is the dominant anion in the seafloor hydrothermal fluids (Von Damm, 1990), its concentration plays a major role in their metal-carrying capacities. Decreased fluid chlorinity (due to a probable sub-seafloor boiling and phase separation) seems to result in the low trace metal concentrations in the studied vent fluids (Cu and majority of REE; Table 8). Particularly, the low REE content (Table 8) supports the

assumption that the sampled Wakamiko Crater vent fluids are the low-chlorinity fractions of phase-separated hydrothermal fluids: (1) REE are non-volatile elements and will separate in the high-chlorinity phase; (2) REE are mainly complexed by Cl^- ions in the hot acidic seafloor hydrothermal fluids (Douville et al., 1999) and will concentrate in the high-chlorinity phase. All this reasonably explains the low concentrations of all the studied trace elements in the Wakamiko Crater stibnite deposits (Table 7). Other possible reasons for this apparent depletion may be the high water/rock ratio, low temperature in the reaction zone, type of source rock, sub-surface precipitation, etc., but given we have insufficient data, any further discussion of this observation would be a mere speculation.

The positive Eu anomaly at the chondrite-normalized REE distribution patterns of the Wakamiko Crater vent fluids (Fig. 9) is typical for the high-temperature seafloor hydrothermal fluids and its origin is discussed elsewhere (Michard et al., 1983; Michard and Albarède, 1986; Michard, 1989; Klinkhammer et al., 1994; Bau and Dulski, 1999; Douville et al., 1999).

Relatively high Fe concentrations (with respect to the other trace metals; Table 7) in the stibnite samples may be explained by the presence of Fe-sulfides (not detected by XRD) in contents below the detection limits of the XRD (~4 wt.%). High Mg and Al concentrations in all the samples (Table 7) likely confirm the assumptions from the XRD studies that talc-smectite is present in the samples (see Mineralogy of the hydrothermal deposits).

Heavy S isotope composition of the Wakamiko Crater vent fluid sulfate: A common feature of the volcanic arc/back-arc systems?

The S isotope composition ($\delta^{34}S$) of seafloor hydrothermal deposits at arc/back-arc settings shows substantial variability (Fig. 11). The wide variation in $\delta^{34}S$ is a result of S isotope fractionation due to four processes contributing to the S budget of the seafloor hydrothermal system: (1) basement rock sulfide supplied though the interaction of hydrothermal fluid with basement rocks (Shanks and Seyfried 1987; Shanks 2001; Ono et al. 2007), (2) thermochemical reduction of sulfate supplied by seawater (Shanks and Seyfried 1987; Shanks 2001; Ono et al. 2007), (3) disproportionation of SO_2 supplied by magmatic vapors (Kusakabe et al. 2000; de Ronde et al. 2005, 2011, 2015; McDermott et al. 2015; Peters et al. 2021), and (4) bacterial

328 sulfate reduction in sediment-covered hydrothermal systems (Aoyama et al. 2014; LaFlamme et
329 al. 2018).

330 Sulfide sulfur in the Wakamiko Crater hydrothermal deposits has an isotope composition
331 ($\delta^{34}S$) within the range of that of the hydrothermal deposits of mid-ocean ridges and back-arc
332 basins, and at the heavy end of the S isotope range of the hydrothermal deposits at volcanic arcs
333 (Fig. 11). It falls between the S isotope composition of the terrestrial mantle sulfide and seawater
334 sulfate, but being closer to the former (Table 7; Fig. 11). However, although the S isotope
335 composition of Wakamiko Crater stibnite-bearing deposits is similar to that of the hydrothermal
336 deposits at mid-ocean ridges, it is unlikely that the terrestrial mantle sulfide (represented in mid-
337 ocean ridge basalts) can be responsible for the S isotope composition of a hydrothermal deposit
338 rooted in volcanic arc basement. Sulfur isotope composition of the studied deposits falls within
339 the range of S isotope composition of the island arc volcanic rocks (IAVR) and is close to
340 $\delta^{34}S_{IAVR}$ mean value (Fig. 11). This suggests that the S bound in the sulfides of the Wakamiko
341 Crater hydrothermal deposits has derived from the volcanic arc basement rocks. The S isotope
342 composition of the studied sulfide (Sb_2S_3) supports the origin of sulfide S in the overall Ryukyu
343 Arc hydrothermal deposits being generally dominated by basement rock S (Fig. 11). There are no
344 clear isotopic indications either for disproportionation of magmatic SO_2 or for microbial sulfate
345 reduction within the Wakamiko Crater sediments, as any of these processes would have driven
346 the $\delta^{34}S$ of produced sulfide to negative values.

347 The heavier S isotope composition of sulfate in the White Cone (Wakamiko Crater) vent
348 fluids ($\delta^{34}S_{sulfate}$ = 21.6 - 22.0 ‰) than that of seawater ($\delta^{34}S_{sulfate}$ = 20.97 ± 0.10 ‰; Paris et al.
349 2013) is similar to the heavy S isotope composition of sulfate in the CLAM (Okinawa Trough;
350 Gamo et al. 1991), Brothers Upper Cone and Macauley (Kermadec Arc; Peters et al. 2021),
351 Niuatahi South-Central, Niuatahi Northern Cone and Niua North (Tonga Arc: Peters et al. 2021)
352 and Daiyon-Yonaguni Knoll (Okinawa Trough; Dekov et al. 2022) hydrothermal fluids ($\delta^{34}S_{sulfate}$
353 > 21.0 ‰) and deserves some consideration.

354 Disproportionation of magmatic SO_2 is invoked to explain the heavy S isotope composition
355 of sulfate ($\delta^{34}S_{sulfate}$ > 20.97 ± 0.10 ‰) in the acid-sulfate fluids ($[SO_4]_{vent\ fluid} > [SO_4]_{seawater}$) of
356 the Tonga-Kermadec Volcanic Arc hydrothermal vents (Peters et al. 2021). However, this
357 mechanism does not seem to be responsible for the heavy S isotope composition of sulfate in

358 non-acid-sulfate hydrothermal fluids ($[SO_4]_{vent\ fluid} < [SO_4]_{seawater}$) like those of the Okinawa
359 Trough and Ryukyu Volcanic Arc vent fields: CLAM (Gamo et al. 1991), Daiyon-Yonaguni
360 Knoll (Suzuki et al. 2008) and Wakamiko Crater (Yamanaka et al. 2013).

361 We know that sulfate reduction in a closed system causes an increase in $\delta^{34}S$ value of the
362 residual sulfate (i.e., removal of the isotopically light sulfide during sulfate reduction) with
363 decreasing sulfate concentration (Ohmoto and Rye 1979; Shanks et al. 1981). Thus, the S isotope
364 composition of the sulfate from the White Cone vent fluids can be interpreted as a result of
365 sulfate reduction. Sulfate reduction or sulfide oxidation depends on the rate of mixing between
366 the hydrothermal fluid and seawater (Peter and Shanks 1992). Slow mixing of the hydrothermal
367 fluid and seawater in the chimney walls or within a mound favors sulfate reduction. This sulfate
368 reduction results in S isotope fractionation approaching equilibrium values and ^{34}S-enriched
369 sulfate resulting from a reservoir effect, as ^{32}S is removed to the sulfide reservoir (Peter and
370 Shanks 1992). Overall, it seems that slow mixing of hydrothermal fluid with seawater within the
371 chimney walls and mounds that favors reduction of the sulfate dissolved in the fluids and results
372 in a heavy S isotope composition of the vent fluid sulfate may be a common process in arc/back-
373 arc settings (Fig. 11). Along with the disproportionation of magmatic SO_2, it contributes to a
374 more heavy S isotope composition of the seawater sulfate and the magnitude of this heavy S
375 source needs to be further evaluated.

376 In the studied case, the S isotope composition of the Wakamiko Crater vent fluids supports
377 the conclusion of the stability phase diagrams modeling that the stibnite has precipitated within
378 the chimney walls and mounds (i.e., as a result of diffused discharge).

379

380 ## IMPLICATIONS

381 Stibnite and metastibnite are the world's main resource for Sb. Our knowledge on their
382 occurrence and mode of formation on the vast seafloor is limited. The study on stibnite and
383 metastibnite presented here seems to be the first modest step in gaining insight into the conditions
384 and mode of formation of these minerals at the seafloor. The results of this investigation suggest
385 that future exploration for stibnite-metastibnite deposits on both the seafloor and continents
386 should focus on volcanic arc and back-arc settings (both modern and ancient), where these two
387 minerals may have massively precipitated under low temperature (<50 °C), low *pH*, and at

slightly reduced to slightly oxic (*Eh* = -0.5 – +0.5 V) hydrothermal conditions. The hydrothermal mounds with their porous structure seem to be suited for stibnite and metastibnite precipitation. Precipitation of stibnite in seafloor hydrothermal conditions should always be accompanied by the precipitation of metastibnite, which we consider is a result of rapid quenching of the hot hydrothermal fluid upon mixing with cold seawater, with rapid mineral precipitation at the stibnite-vent fluid interface. As the studied stibnite and metastibnite proved to have low concentrations of all the analyzed trace elements, the future surveys for stibnite-metastibnite deposits do not need to consider these deposits as possible resource for valuable bi-products.

Sulfur isotope study of the hydrothermal fluids precipitating stibnite-metastibnite implies that sulfate reduction within the porous hydrothermal mounds may be a common process at volcanic arc/back-arc hydrothermal settings. This geochemical detail needs to be considered in future interpretations of the mineralogy and geochemistry of massive hydrothermal deposits formed on the seafloor.

ACKNOWLEDGEMENTS

Our sincere thanks go to Mrs. M. Sudama (Tokyo University of Marine Science and Technology) for helping us with the EMP analyses. We highly appreciate the efforts and time sacrificed by the Associate Editor David Dolejš, Cornel de Ronde and an anonymous reviewer to carefully read the paper and give us valuable suggestions and comments, which significantly improved it.

REFERENCES CITED

Alibo, D.S., and Nozaki, Y. (1999) Rare earth elements in seawater: particle association, shale-normalization, and Ce oxidation. Geochimica et Cosmochimica Acta, 63, 363-372.

Alt, J.C., Shanks, W.C. III, and Jackson, M.C. (1993) Cycling of sulfur in subduction zones: The geochemistry of sulfur in the Mariana Island Arc and back-arc trough. Earth and Planetary Science Letters, 119, 477-494.

Alt, J.C., Teagle, D.A.H., Brewer, T.S., Shanks, W.C. III, and Halliday, A.N. (1998) Alteration and mineralization of an oceanic forearc and the ophiolite-ocean crust analogy. Journal of Geophysical Research, 103, 12,365-12,380.

Aoyama, S., Nishizawa, M., Takai, K., and Ueno, Y. (2014) Microbial sulfate reduction within the Iheya North subseafloor hydrothermal system constrained by quadruple sulfur isotopes. Earth and Planetary Science Letters, 398, 113-126.

Aramaki, S. (1984) Formation of the Aira Caldera, Southern Kyushu, ~22,000 years ago. Journal of Geophysical Research, 89, 8485-8501.

Arnold, M., and Sheppard, S.M.F. (1981) East Pacific Rise at latitude 21°N: isotopic composition and origin of the hydrothermal sulfur. Earth and Planetary Science Letters, 56, 148-156.

Bau, M., and Dulski, P. (1999) Comparing yttrium and rare earths in hydrothermal fluids from the Mid-Atlantic Ridge: Implications for Y and REE fractionation during near-vent mixing and for the Y/Ho ratio of Proterozoic seawater. Chemical Geology, 155, 77-90.

Becker, G.F. (1888) Geology of the Quicksilver Deposits of the Pacific Slope. Chapter 11. Descriptive geology of the Steamboat Springs district. Monographs of the United States Geological Survey, 13, 331-353.

Berkenbosch, H.A., de Ronde, C.E.J., Gemmell, J.B., McNeill, A.W., and Goemann, K. (2012) Mineralogy and Formation of Black Smoker Chimneys from Brothers Submarine Volcano, Kermadec Arc. Economic Geology, 107, 1613-1633.

Bluth, G.J., and Ohmoto, H. (1988) Sulfide-sulfate chimneys on the East Pacific Rise, 11° and 13°N latitudes. Part II: Sulfur isotopes. The Canadian Mineralogist, 26, 505-515.

Brookins, D.G. (1970) Mineralogical notes: metastibnite from The Geysers, Sonoma County, California. American Mineralogist, 55, 2103-2104.

Brown, K. (2011) Antimony and arsenic sulfide scaling in geothermal binary plants. Proceedings International Workshop on Mineral Scaling, Manila, Philippines, 25-27 May 2011, 103-106.

Butler, I.B., Fallick, A.E., and Nesbitt, R.W. (1998) Mineralogy, sulphur isotope geochemistry and the development of sulphide structures at the Broken Spur hydrothermal vent site, 29°10´N, Mid-Atlantic Ridge. Journal of the Geological Society of London, 155, 773-785.

de Hoog, J.C.M., Taylor, B.E., and van Bergen, M.J. (2001) Sulfur isotope systematics of basaltic lavas from Indonesia: implications for the sulfur cycle in subduction zones. Earth and Planetary Science Letters, 189, 237-252.

Dekov, V.M., and Savelli, C. (2004) Hydrothermal activity in the SE Tyrrhenian Sea: An overview of 30 years of research. Marine Geology, 204, 161-185.

Dekov, V.M., Kyono, K., Yasukawa, K., Guéguen, B., Ivarsson, M., Kamenov, G.D., Yamanaka, T., Asael, D., Ishida, M., Cavalcante, L.L., Kato, Y., Toki, T., and Ishibashi, J.-I. (2022) Mineralogy, geochemistry and microbiology insights into precipitation of stibnite and orpiment at the Daiyon-Yonaguni Knoll (Okinawa Trough) hydrothermal barite deposits. Chemical Geology, 610, 121092.

de Ronde, C.E.J., Faure, K., Bray, C.J., Chappell, D.A., and Wright, I.C. (2003) Hydrothermal fluids associated with seafloor mineralization at two southern Kermadec arc volcanoes, offshore New Zealand. Mineralium Deposita, 38, 217-233.

de Ronde, C.E.J., Hannington, M.D., Stoffers, P., Wright, I.C., Ditchburn, R.G., Reyes, A.G., Baker, E.T., Massoth, G.J., Lupton, J.E., Walker, S.L., Greene, R.R., Soong, C.W.R., Ishibashi, J., Lebon, G.T., Bray, C.J., and Resing, J.A. (2005) Evolution of a submarine magmatic-hydrothermal system: Brothers volcano, southern Kermadec Arc, New Zealand. Economic Geology, 100, 1097-1133.

de Ronde, C.E.J., Massoth, G.J., Butterfield, D.A., Christenson, B.W., Ishibashi, J., Ditchburn, R.G., Hannington, M.D., Brathwaite, R.L., Lupton, J.E., Kamenetsky, V.S., Graham, I.J., Zellmer, G.F., Dziak, R.P., Embley,

R.W., Dekov, V.M., Munnik, F., Lahr, J., Evans, L.J., and Takai, K. (2011) Submarine hydrothermal activity and gold-rich mineralization at Brothers Volcano, Kermadec Arc, New Zealand. Mineraluim Deposita, 46, 541-584.

de Ronde, C.E.J., Chadwick Jr, W.W., Ditchburn, R.G., Embley, R.W., Tunnicliffe, V., Baker, E.T., Walker, S.L., Ferrini, V.L., and Merle, S.M. (2015) Molten sulfur lakes of intraoceanic arc volcanoes. In: Rouwet, D., Christenson, B., Tassi, F., Vandemeulebrouck, J. (Eds), Volcanic Lakes, Advances in Volcanology, Springer-Verlag, Berlin Heidelberg, pp. 261-288.

Douville, E., Bienvenu, P., Charlou, J.L., Donval, J.P., Fouquet, Y., Appriou, P., and Gamo, T. (1999) Yttrium and rare earth elements in fluids from various deep-sea hydrothermal systems. Geochimica et Cosmochimica Acta, 63, 627-643.

Duckworth, R.C., Knott, R., Fallick, A.E., Rickard, D., Murton, B.J., and van Dover, C. (1995) Mineralogy and sulphur isotope geochemistry of the Broken Spur sulphides, 29°N, Mid-Atlantic Ridge. In: Parson, L.M., Walker, C.L., Dixon, D.R. (Eds.), Hydrothermal Vents and Processes. Geological Society Special Publication, 87, 175-189.

Firstova, A., Stepanova, T., Cherkashov, G., Goncharov, A., and Babaeva, S. (2016) Composition and formation of gabbro-peridotite hosted seafloor massive sulfide deposits from the Ashadze-1 hydrothermal field, Mid-Atlantic Ridge. Minerals, 6, 19.

Fouquet, Y., Knott, R., Cambon, P., Fallick, A., Rickard, D., and Desbruyeres, D. (1996) Formation of large sulfide mineral deposits along fast spreading ridges. Example from off-axial deposits at 12°43´N on the East Pacific Rise. Earth and Planetary Science Letters, 144, 147-162.

Fujiwara, T., Toyoda, S., Uchida, A., Ishibashi, J., Nakai, S., and Takamasa, A. (2015) ESR dating of barite in sea-floor hydrothermal sulfide deposits in the Okinawa Trough. In: Ishibashi, J., et al. (Eds), Subseafloor Biosphere Linked to Hydrothermal Systems: TAIGA Concept, pp. 369-386.

Gamo, T., Sakai, H., Kim, E-S., Shitashima, K., and Ishibashi, J.-I. (1991) High alkalinity due to sulfate reduction in the CLAM hydrothermal field, Okinawa Trough. Earth and Planetary Science Letters, 107, 328-338.

Gemmell, J.B., and Sharpe, R. (1998) Detailed sulfur-isotope investigation of the TAG hydrothermal mound and stockwork zone, 26°N, Mid-Atlantic Ridge. In: Herzig, P.M., Humphris, S.E., Miller, D.J., Zierenberg, R.A. (Eds.), Proc. ODP, Sci. Results, College Station, TX, 158, pp. 71-84.

Gena, K., Chiba, H., and Kase, K. (2005) Tin-bearing chalcopyrite and platinum-bearing bismuthinite in the active Tiger chimney, Yonaguni Knoll IV seafloor hydrothermal system, South Okinawa Trough, Japan. Earth Science Reports, Okayama University, 12, 1-5.

German, C.R., and Von Damm, K.L. (2003) Hydrothermal processes. In: Turekian, K.K., Holland, H.D. (Eds), *Treatise on Geochemistry,* Vol. 6 The Oceans and Marine Geochemistry, Elsevier, Oxford, pp. 181-222.

Halbach, P., Pracejus, B., and Märten, A. (1993) Geology and mineralogy of massive sulfide ores from the central Okinawa Trough, Japan. Economic Geology, 88, 2210-2225.

Hannington, M.D., and Scott, S.D. (1988) Mineralogy and geochemistry of an hydrothermal silica-sulfide-sulfate spire in the caldera of Axial-Seamount, Juan de Fuca Ridge. The Canadian Mineralogist, 26, 603-625.

Harigane, Y. (2015) Structural development of volcanic caldera in Kume-jima western offshore. R/V Natsushima NT14–22 Cruise Report, Japan Agency for Marine-Earth Science and Technology, Yokosuka, Japan, p. 24.

Hayasaka, S. (1987) Geologic structure of Kagoshima Bay, south Kyushu, Japan. Monograph of the Association for the Geological Collaboration in Japan, 33, 225-233. (in Japanese with English abstract)

Hekinian, R., Fevrier, H., Bischoff, J.L., Picot, P., and Shanks, W.C. (1980) Sulfide deposits from the East Pacific Rise near 21°N. Science, 207, 1433-1444.

Herzig, P.M., Petersen, S., and Hannington, M.D. (1998) Geochemistry and sulfur-isotopic composition of the TAG hydrothermal mound, Mid-Atlantic Ridge, 26°N. In: Herzig, P.M., Humphris, S.E., Miller, D.J., Zierenberg, R.A. (Eds.), Proc. ODP, Sci. Results, College Station, TX, 158, pp. 47-70.

Hunt, S. (1888) The classification and nomenclature of metalline minerals. Proceedings of the American Philosophical Society, 25, 170-180.

Kase, K., Yamamoto, M., and Shibata, T. (1990) Copper-rich sulfide deposit near 23°N, Mid-Atlantic Ridge: chemical composition, mineral chemistry, and sulfur isotopes. In: Detrick, R., Honnorez, J., Bryan, W.B., Juteau, T., et al. (Eds.), Proc. ODP, Sci. Results, College Station, TX, 106/109, pp. 163-177.

Kawasumi, S., Chiba, H., and Ishibashi, J. (2016) Sulfur systematics in the Izena Hole seafloor hydrothermal systems, Okinawa Trough: Stable isotope, mineralogy and redox equilibria. Japan Geoscience Union meeting 2016, May 22-26, Makuhari Messe.

Kerridge, J.F., Haymon, R.M., and Kastner, M. (1983) Sulfur isotope systematics at the 21°N site, East Pacific Rise. Earth and Planetary Science Letters, 66, 91-100.

Kim, J., Lee, I., and Lee, K.-Y. (2004) S, Sr, and Pb isotopic systematic of hydrothermal chimney precipitates from the Eastern Manus Basin, western Pacific: Evaluation of magmatic contribution to hydrothermal system. Journal of Geophysical Research, 109, B12210.

Kim, J., Lee, K.-Y., and Kim, J.-H. (2011) Metal-bearing molten sulfur collected from a submarine volcano: Implications for vapor transport of metals in seafloor hydrothermal systems. Geology, 39, 351-354.

Klinkhammer, G.P., Elderfield, H., Edmond, J.M., and Mitra, A. (1994) Geochemical implications of rare earth element patterns in hydrothermal fluids from mid-ocean ridges. Geochimica et Cosmochimica Acta, 58, 5105-5113.

Knott, R., Fallick, A.E., Rickard, D., and Bäcker, H. (1995) Mineralogy and sulphur isotope characteristics of a massive sulphide boulder, Galapagos Rift, 85°55´W. In: Parson, L.M., Walker, C.L., Dixon, D.R. (Eds.), Hydrothermal Vents and Processes. Geological Society Special Publication, 87, 207-222.

Konno, U., Tsunogai, U., Nakagawa, F., Nakaseama, M., Ishibashi, J.-I., Nunoura, T., and Nakamura, K. (2006) Liquid CO_2 venting on the seafloor: Yonaguni Knoll IV hydrothermal system, Okinawa Trough. Geophysical Research Letters, 33, L16607.

Kusakabe, M., Mayeda, S., and Nakamura, E. (1990) S, O and Sr isotope systematics of active vent materials from the Mariana backarc basin spreading axis at 18°N. Earth and Planetary Science Letters, 100, 275-282.

Kusakabe, M., Komoda, Y., Takano, B., and Abiko, T. (2000) Sulfur isotopic effects in the disproportionation reaction of sulfur dioxide in hydrothermal fluids: implications for the $\delta^{34}S$ variations of dissolved bisulfate and elemental sulfur from active crater lakes. Journal of Volcanology and Geothermal Research, 97, 287-307.

Kyono, A., and Kimata, M. (2004) Structural variations induced by difference of the inert pair effect in the stibnite-bismuthinite solid solution series $(Sb,Bi)_2S_3$. American Mineralogist, 89, 932-940.

Labidi, J., Cartigny, P., Birck, J.L., Assayag, N., and Bourrand, J.J. (2012) Determination of multiple sulfur isotopes in glasses: A reappraisal of the MORB $\delta^{34}S$. Chemical Geology, 334, 189-198.

LaFlamme, C., Hollis, S.P., Jamieson, J.W., and Fiorentini, M.L. (2018) Three-dimensional spatially constrained sulfur isotopes highlight processes controlling sulfur cycling in the near surface of the Iheya North hydrothermal system, Okinawa Trough. Geochemistry, Geophysics, Geosystems, 19, 2798-2812.

Lafuente, B., Downs, R.T., Yang, H., and Stone, N. (2015) The power of databases: The RRUFF project. In: Armbruster, T., Danisi, R.M. (Eds.), Highlights in Mineralogical Crystallography, De Gruyter, Berlin, pp. 1-30.

Lüders, V., Pracejus, B., and Halbach, P. (2001) Fluid inclusion and sulfur isotope studies in probable modern analogue Kuroko-type ores from the JADE hydrothermal field (Central Okinawa Trough, Japan). Chemical Geology, 173, 45-58.

Marchig, V., Puchelt, H., Rösch, H., and Blum, N. (1990) Massive sulfides from ultra-fast spreading ridge, East Pacific Rise at 18-21°S: A geochemical stock report. Marine Mining, 9, 459-493.

Matsumoto, T., Kinoshita, M., Nakamura, M., Sibuet, J.-C., Lee, C.-S., Hsu, S.-K., Oomori, T., Shinjo, R., Hashimoto, Y., Hosoya, S., Imamura, M., Ito, M., Tukuda, K., Yagi, H., Tatekawa, K., Kagaya, I., Hokakubo, S., Okada, T., and Kimura, M. (2001) Volcanic and hydrothermal activities and possible "segmentation" of the axial rifting in the westernmost part of the Okinawa Trough – preliminary results from the YOKOSUKA/SHINKAI 6500 Lequios Cruise, JAMSTEC Journal of Deep-Sea Research, 19, 95-107. (in Japanese with English abstract).

McDermott, J.M., Ono, S., Tivey, M.K., Seewald, J.S., Shanks, W.C., and Solow, A.R. (2015) Identification of sulfur sources and isotopic equilibria in submarine hot-springs using multiple sulfur isotopes. Geochimica et Cosmochimica Acta, 160, 169-187.

McDonough, W.F., and Sun, S.-s. (1995) The composition of the Earth. Chemical Geology, 120, 223-253.

Melekestseva, I.Yu. (2010) Sulfur isotopic composition of massive sulfides from the Semenov hydrothermal cluster, 13°31´N, MAR. Minerals of the Ocean-5 and Deep-Sea Minerals and Mining-2 Joint International Conference, St. Petersburg, Russia, 28 June – 01 July 2010, Abstract Volume, pp. 70-73.

Michard, A. (1989) Rare earth element systematics in hydrothermal fluids. Geochimica et Cosmochimica Acta, 53, 745-750.

Michard, A., and Albarède, F. (1986) The REE content of some hydrothermal fluids. Chemical Geology, 55, 51-60.

Michard, G., Albarède, F., Michard, A., Minster, J.F., and Charlou, J.L. (1983) Rare-earth elements and uranium in high-temperature solutions from East Pacific Rise hydrothermal vent field (13 °N). Nature, 303, 795-797.

Minami, H., and Ohara, Y. (2017) The Gondou hydrothermal field in the Ryukyu Arc: A huge hydrothermal system on the flank of a caldera volcano. Geochemistry, Geophysics, Geosystems, 18, 3489-3516.

Mozgova, N.N., Borodaev, Yu.S., Tsepin, A.I., and Yankovich, S. (1977) New data on metastibnite. Proceedings of USSR Academy of Sciences, 237, 4, 937-940. (in Russian)

Nakashima, K., Sakai, H., Yoshida, H., Chiba, H., Tanaka, Y., Gamo, T., Ishibashi, J.-I., and Tsunogai, U. (1995) Hydrothermal mineralization in the Mid-Okinawa Trough. In: Sakai, H., Nozaki, Y. (Eds), Biogeochemical Processes and Ocean Flux in the Western Pacific. Terra Scientific Publishing Company, Tokyo, pp. 487-508.

Nedachi, M., Ueno, H., Oki, K., Shiga, Y., Hayasaka, S., Ossaka, J., Nogami, K., Ito, N., and Hashimoto, J. (1991) Sulfide veinlets and the surrounding marine sediments in the fumarole area in the Wakamiko Caldera, northern Kagoshima Bay. JAMSTEC Journal of Deep-Sea Research, 7, 235-243.

Nishio, R., and Chiba, H. (2012) Mineralogical and sulfur stable isotopic study of mineralization at the No.4 Yonaguni Knoll seafloor hydrothermal system, Okinawa Trough. Annual Meeting of the Geochemical Society of Japan, Abstracts, Geochemical Society of Japan, 59.

Nozaki, T., Ishibashi, J.-I., Shimada, K., Nagase, T., Takaya, Y., Kato, Y., Kawagucci, S., Watsuji, T., Shibuya, T., Yamada, R., Saruhashi, T., Kyo, M., and Takai, K. (2016) Rapid growth of mineral deposits at artificial seafloor hydrothermal vents. Scientific Reports, 6, 22163.

Ohmoto, H., and Rye, R.O. (1979) Isotopes of sulfur and carbon. In: Barnes, H.L. (Ed.), Geochemistry of Hydrothermal Ore Deposits, Wiley, New York, pp. 509-567.

Okamoto, K., Ishibashi, J.-I., Motomura, Y., Yamanaka, T., and Fujikura, K. (2002) Mineralogical studies of hydrothermal deposits collected from the Daiyon-Yonaguni Knoll and the Hatoma Knoll in the Okinawa Trough. JAMSTEC Journal of Deep-Sea Research, 21, 75-81. (in Japanese with English abstract).

Ôki, K., and Hayasaka, S. (1978) Geological study on Kagoshima Bay, South Kyushu, Japan. Part IV - A Note on the Peculiar Mode of Occurrence of Foraminifers in the Bottom Sediments of the Bay-head Area. Reports of the Faculty of Science, Kagoshima University (Earth Science and Biology), 11, 1-16.

Olivier-Fourcade, J., Maurin, M., and Philippot, E. (1983) Étude cristallochimique de système Li_2S-Sb_2S_3. Revue de Chimie Minérale, 20, 196-213.

Ono, S., Shanks III, W.C., Rouxel, O.J., and Rumble, D. (2007) S-33 constraints on the seawater sulfate contribution in modern seafloor hydrothermal vent sulfides. Geochimica et Cosmochimica Acta, 71, 1170-1182.

Ooki, M., Miyoshi, Y., Shimada, K., Ishibashi, J.-I., and Nozaki, T. (2012) Mineralogy and geochemistry of hydrothermal ores collected from active hydrothermal fields in shallow water depth. Proceedings of Japan Geoscience Union Meeting 2012, BBG21-P09 (Abstract).

Paris, G., Sessions, A.L., Subhas, A.V., and Adkins, J.F. (2013) MC-ICP-MS measurement of $\delta^{34}S$ and $\Delta^{33}S$ in small amounts of dissolved sulfate. Chemical Geology, 345, 50-61.

Peter, J.M., and Shanks, W.C. III (1992) Sulfur, carbon, and oxygen isotope variations in submarine hydrothermal deposits of Guaymas Basin, Gulf of California, USA. Geochimica et Cosmochimica Acta, 56, 2025-2040.

Peters, C., Strauss, H., Haase, K., Bach, W., de Ronde, C.E.J., Kleint, C., Stucker, V., and Diehl, A. (2021) SO_2 disproportionation impacting hydrothermal sulfur cycling: Insights from multiple sulfur isotopes for

603 hydrothermal fluids from the Tonga-Kermadec intraoceanic arc and the NE Lau Basin. Chemical Geology,
604 586, 120586.
605 Peters, M., Strauss, H., Farquhar, J., Ockert, C., Eickmann, B., and Jost, C.L. (2010) Sulfur cycling at the Mid-
606 Atlantic Ridge: A multiple sulfur isotope approach. Chemical Geology, 269, 180-196.
607 Peters, M., Strauss, H., Petersen, S., Kummer, N.-A., and Thomazo, C. (2011) Hydrothermalism in the Tyrrhenian
608 Sea: Inorganic and microbial sulfur cycling as revealed by geochemical and multiple sulfur isotope data.
609 Chemical Geology, 280, 217-231.
610 Petersen, S., Herzig, P.M., Hannington, M.D., Jonasson, I.R., and Arribas, JR. A. (2002) Submarine gold
611 mineralization near Lihir Island, New Ireland fore-arc, Papua New Guinea. Economic Geology, 97, 1795-
612 1813.
613 Petersen, S., Monecke, T., Westhues, A., Hannington, M.D., Gemmell, J.B., Sharpe, R., Peters, M., Strauss, H.,
614 Lackschewitz, K., Augustin, N., Gibson, H., and Kleeberg, R. (2014) Drilling shallow-water massive sulfides
615 at the Palinuro Volcanic Complex, Aeolian Island Arc, Italy. Economic Geology, 109, 2129-2158.
616 Rouxel, O., Fouquet, Y., and Ludden, J.N. (2004) Copper isotope systematics of the Lucky Strike, Rainbow, and
617 Logatchev sea-floor hydrothermal fields on the Mid-Atlantic Ridge. Economic Geology, 99, 585-600.
618 Sakamoto, H. (1985) The distribution of mercury, arsenic, and antimony in sediments of Kagoshima Bay. Bulletin of
619 the Chemical Society of Japan, 58, 580-587.
620 Shanks, W.C. (2001) Stable isotopes in seafloor hydrothermal systems: Vent fluids, hydrothermal deposits,
621 hydrothermal alteration, and microbial processes. In: Valley, J.W., Cole, D.R. (Eds), Stable Isotope
622 Geochemistry. Reviews in Mineralogy and Geochemistry, 43, pp. 469-525.
623 Shanks, W.C. III, Bischoff, J.L., and Rosenbauer, R.J. (1981) Seawater sulfate reduction and sulfur isotope
624 fractionation in basaltic systems: Interaction of seawater with fayalite and magnetite at 200-350°C.
625 Geochimica et Cosmochimica Acta, 45, 1977-1995.
626 Shanks, W.C. III, Koski, R.A., and Woodruff, L.G. (1984) Mineralogy and stable isotope systematics of sulfide
627 deposits from the Juan de Fuca Ridge. EOS, 65, 1113.
628 Shanks, W.C. III, and Seyfried, W.E. Jr. (1987) Stable isotope studies of vent fluids and chimney minerals, southern
629 Juan de Fuca Ridge. Sodium metasomatism and seawater sulfate reduction. Journal of Geophysical Research,
630 92, 11387-11399.
631 Skirrow, R., and Coleman, M.L. (1982) Origin of sulfur and geothermometry of hydrothermal sulfides from the
632 Galapagos Rift, 86°N. Nature, 299, 142-144.
633 Stuart, F.M., Turner, G., Duckworth, R.C., and Fallick, A.E. (1994) Helium isotopes as tracers of trapped
634 hydrothermal fluids in ocean-floor sulfides. Geology, 22, 823-826.
635 Stuart, F.M., Harrop, P.J., Knott, R., Fallick, A.E., Turner, G., Fouquet, Y., and Rickard, D. (1995) Noble gas
636 isotopes in 25 000 years of hydrothermal fluids from 13°N on the East Pacific Rise. In: Parson, L.M., Walker,
637 C.L., Dixon, D.R. (Eds.), Hydrothermal Vents and Processes. Geological Society Special Publication, 87,
638 133-143.

Styrt, M.M., Brackmann, A.J., Holland, H.D., Clark, B.C., Pisutha-Arnold, V., Eldridge, C.S., and Ohmoto, H. (1981) The mineralogy and the isotopic composition of sulfur in hydrothermal sulfide/sulfate deposits on the East Pacific Rise, 21°N latitude. Earth and Planetary Science Letters, 53, 382-390.

Suzuki, R., Ishibashi, J., Nakaseama, M., Konno, U., Tsunogai, U., Gena, K., and Chiba, H. (2008) Diverse range of mineralization induced by phase separation of hydrothermal fluid: Case study of the Yonaguni Knoll IV hydrothermal field in the Okinawa Trough back-arc basin. Resource Geology, 58, 267-288.

Ueda, A., and Sakai, H. (1984) Sulfur isotope study of Quaternary volcanic rocks from the Japanese Islands Arc. Geochimica et Cosmochimica Acta, 48, 1837-1848.

Ueno, H., Hamasaki, H., Murakawa, Y., Kitazono, S., and Takeda, T. (2003) Ore and gangue minerals of sulfide chimneys from the North Knoll, Iheya Ridge, Okinawa Trough, Japan. JAMSTEC Journal of Deep-Sea Research, 22, 49-62.

Von Damm, K.L. (1990) Seafloor hydrothermal activity: Black smoker chemistry and chimneys. Annual Review of Earth and Planetary Sciences, 18, 173-204.

Warr, L.N. (2021) IMA–CNMNC approved mineral symbols. Mineralogical Magazine, 85, 291-320.

Wilson, N., Webster-Brown, J., and Brown, K. (2007) Controls on stibnite precipitation at two New Zealand geothermal power stations. Geothermics, 36, 330-347.

Woodhead, J.D., Harmon, R.S., and Fraser, D.G. (1987) O, S, Sr, and Pb isotope variations in volcanic rocks from the Northern Mariana Islands: implications for crustal recycling in intra-oceanic arcs. Earth and Planetary Science Letters, 83, 39-52.

Woodruff, L.G., and Shanks, W.C., III. (1988) Sulfur isotope study of chimney minerals and vent fluids from 21°N, East Pacific Rise: Hydrothermal sulfur sources and disequilibrium sulfate reduction. Journal of Geophysical Research, 93, 4562-4572.

Yamanaka, T., Maeto, K., Akashi, H., Ishibashi, J.-I., Miyoshi, Y., Okamura, K., Noguchi, T., Kuwahara, Y., Toki, T., Tsunogai, U., Ura, T., Nakatani, T., Maki, T., Kubokawa, K., and Chiba, H. (2013) Shallow submarine hydrothermal activity with significant contribution of magmatic water producing talc chimneys in the Wakamiko Crater of Kagoshima Bay, southern Kyushu, Japan. Journal of Volcanology and Geothermal Research, 258, 74-84.

Yang, B., Liu, J., Shi, X., Zhang, H., Wang, X., Wu, Y., and Fang, X. (2020) Mineralogy and sulfur isotope characteristics of metalliferous sediments from the Tangyin hydrothermal field in the southern Okinawa Trough. Ore Geology Reviews, 120, 103464.

Zierenberg, R.A., Shanks, W.C., III., and Bischoff, J.L. (1984) Massive sulfide deposits at 21°N, East Pacific Rise: chemical composition, stable isotopes, and phase equilibria. Geological Society of America Bulletin, 95, 922-929.

Figure captions

675

676 **FIGURE 1.** Locations of: (**a**) the Wakamiko Crater (Kagoshima Bay, southern Kyushu Island,
677 Ryukyu Arc), Daisan-Kume Knoll (Ryukyu Arc) and Daiyon-Yonaguni Knoll (Okinawa
678 Trough), and (**b**) the White Cone and Hairy Cone hydrothermal sites within the Wakamiko
679 Crater.

680

681 **FIGURE 2.** Photographs (taken by the ROV *Hyper-Dolphin*) of the Wakamiko Crater sample
682 sites: (**a**) Hairy Cone chimney and mound from which samples H#893 GE1 and H#893 GE2 were
683 collected; (**b**) White Cone chimney and mound from which sample H#886 GE3 was collected.

684

685 **FIGURE 3.** General views of the studied samples: (**a**) sample H#893 GE1 (Hairy Cone vent); (**b**)
686 sample H#893 GE2 (Hairy Cone vent); (**c**) sample H#886 GE3 (White Cone vent).

687

688 **FIGURE 4.** (**a**) XRD pattern of sample H#893 GE1 (Wakamiko Crater) showing the presence of
689 stibnite (all major XRD peaks) and possibly talc-smectite (T-S). The segment between 55.5 and
690 57.0 º2θ (highlighted by the red rectangular box) was further X-ray scanned with small steps
691 (0.02 º2θ) and slow speed (12 s/step) to reveal the presence of the major XRD peaks of
692 metastibnite. The XRD pattern received is shown at (**b**) along with those of samples H#893 GE2
693 and H#886 GE3, metastibnite (Lafuente et al. 2015) and stibnite (Kyono and Kimata 2004)
694 recorded along the same 55.5 - 57.0 º2θ segment. For comparison, the stibnite-containing
695 samples from the Daisan-Kume Knoll and Daiyon-Yonaguni Knoll sites were analyzed with the
696 same XRD conditions and the XRD patterns are given in (**c**) and (**d**), respectively. Note: to fit the
697 vertical scales of the XRD patterns, the peak intensities (in cps) for metastibnite and stibnite were
698 multiplied by 5 and shifted up by 400 in (**b**) and (**c**), multiplied by 5 and shifted up by 200 in (**d**),
699 whereas the peak Intensities (in cps) for sample 2K1267 L1 were divided by 10 in (**d**).

700

701 **FIGURE 5.** Photomicrographs of stibnite (Sbn) and metastibnite (Msbn) from the studied seafloor
702 hydrothermal deposits (thin polished sections, optical microscope): prismatic stibnite crystals (**a**:
703 reflected plain-polarized light) and (**b**: reflected cross-polarized light) (sample H#893 GE2); all
704 stibnites that were confirmed by XRD have highly unusual pinkish to dark purple anisotropy

colours (normally, stibnite has a brown to blue grey anisotropy); rosettes of acicular crystals (**c**: reflected plain-polarized light) with red internal reflections (**d**: reflected cross-polarized light) (sample H#886 GE3) possibly represent a transitional stage between stibnite and metastibnite at the crystal terminations; in contrast to metastibnite with its red internal reflections, "normal" stibnite would be completely opaque; examples of larger, coarse-grained rosettes of what is shown above (**e** and **g**: reflected plain-polarized light) but with a more pronounced transparency throughout individual crystals (**f** and **h**: red internal reflections, reflected cross-polarized light) (sample H#893 GE1). At this point, the reason for the atypical optical behaviour of a stibnite with characteristics from metastibnite remains speculation (intergrown subdomains of both minerals?); at the JADE seafloor hydrothermal deposit, typical stibnite exists in conjunction with fibrous material similar to the rosettes displayed here (compare Halbach et al. 1993).

FIGURE 6. SEM photomicrographs (SEI) of stibnite from the studied seafloor hydrothermal deposits: (**a**) general view of a rosette of long prismatic stibnite crystals (sample H#893 GE2); (**b**) close up of a prismatic stibnite crystal (sample H#893 GE1); (**c**) thin, long stibnite crystals (sample H#893 GE2).

FIGURE 7. X-ray maps and BSE image of prismatic stibnite (Sbn) in the studied seafloor hydrothermal deposits (sample H#893 GE2): (**a**) X-ray scan in S *K*α; (**b**) X-ray scan in Sb *L*α; (**c**) X-ray scan in As *L*α; (**d**) BSE image. Color scales (right-hand side), elemental concentrations.

FIGURE 8. X-ray maps and BSE image of a rosette of needle-like stibnite (Sbn) in the studied seafloor hydrothermal deposits (sample H#893 GE1): (**a**) X-ray scan in S *K*α; (**b**) X-ray scan in Sb *L*α; (**c**) X-ray scan in As *L*α; (**d**) BSE image. Color scales (right-hand side), elemental concentrations.

FIGURE 9. CI chondrite-normalized (McDonough and Sun 1995) REE distribution patterns of the studied vent fluids from the Wakamiko Crater hydrothermal field (Ryukyu Arc). NPDW = North Pacific Deep Water (Alibo and Nozaki 1999).

735 **FIGURE 10.** Stability phase diagrams for the chemical species (dissolved and solid) in the 687R1
736 vent fluid from the White Cone vent (Wakamiko Crater, Ryukyu Arc): (**a**), (**b**), (**c**) and (**d**) -
737 $\log_{10}a$-$\log_{10}a$ diagrams calculated for $H_2S_{(aq)}$ and $HSb_2S_4^-$; (**e**), (**f**), (**g**) and (**h**) - $\log_{10}a$-$\log_{10}a$
738 diagrams calculated for $H_2S_{(aq)}$ and $Sb(OH)_{3(aq)}$; (**i**), (**j**), (**k**) and (**l**) - $\log_{10}a$-*Eh* diagrams
739 calculated for $H_2S_{(aq)}$. Diagrams were calculated at the venting temperature (177.6 °C; **a**, **e**, **i**) and
740 decreasing temperatures.
741
742 **FIGURE 11.** Sulfur-isotope composition (range) of selected hydrothermal deposits from mid-
743 ocean ridges [unsedimented (mafic- and ultramafic-hosted) and sedimented], volcanic arcs and
744 back-arc basins compared to those of studied stibnite-containing deposits and vent fluids (sulfate
745 S) from the Wakamiko Crater. References: terrestrial mantle (Labidi et al. 2012), island arc
746 volcanic rocks [Japanese Island Arc (Ueda and Sakai 1984), Mariana Island Arc (Woodhead et
747 al. 1987; Alt et al., 1993), Indonesia Island Arc (de Hoog et al. 2001); dark grey strip = range of
748 mean values], seawater (Paris et al. 2013), Galapagos Rift (Skirrow and Coleman 1982; Knott et
749 al. 1995), 21°N EPR (Hekinian et al. 1980; Arnold and Sheppard 1981; Styrt et al. 1981;
750 Kerridge et al. 1983; Zierenberg et al. 1984; Woodruff and Shanks 1988; Stuart et al. 1994), 11-
751 13°N EPR (Bluth and Ohmoto 1988; Stuart et al. 1995; Fouquet et al. 1996; Ono et al. 2007), 9-
752 10°N EPR (Ono et al. 2007), 18-21°S EPR (Marchig et al. 1990; Ono et al. 2007), Lucky Strike
753 (Rouxel et al. 2004; Ono et al. 2007), Broken Spur (Duckworth et al. 1995; Butler et al. 1998),
754 TAG (Stuart et al. 1994; Gemmell and Sharpe 1998; Herzig et al. 1998; Shanks 2001), Snakepit
755 (Kase et al. 1990; Stuart et al. 1994), Southern MAR (Peters et al. 2010), Rainbow (Rouxel et al.
756 2004), Logatchev (Rouxel et al. 2004; Peters et al. 2010), Semenov (Melekestseva 2010), Red
757 Sea (Shanks 2001), Juan de Fuca (Shanks et al. 1984; Shanks and Seyfried 1987; Hannington and
758 Scott 1988; Stuart et al. 1994), Escanaba Trough (Shanks 2001), Guaymas Basin (Shanks 2001),
759 Okinawa Trough (Lüders et al. 2001; Ueno et al. 2003; Nishio and Chiba 2012; Kawasumi et al.
760 2016; Yang et al. 2020; Dekov et al. 2022), Manus Basin (Kim et al. 2004), Kermadec Arc (de
761 Ronde et al. 2005; 2011), Mariana Trough (Kusakabe et al. 1990), Lau Basin (Kim et al. 2011),
762 Izu-Bonin Arc (Alt et al. 1998), Aeolian Arc (Peters et al. 2011; Petersen et al. 2014), Ryukyu
763 Arc (Yamanaka unpublished data for Daisan-Kume Knoll, Hatoma Knoll and Tarama Knoll),
764 Kermadec Arc vent fluids (sulfate S) (Peters et al. 2021), Tonga Arc vent fluids (sulfate S)

765 (Peters et al. 2021), Daiyon-Yonaguni Knoll vent fluids (sulfate S) (Dekov et al. 2022), CLAM
766 vent fluids (sulfate S) (Gamo et al. 1991).
767

TABLE 1. Hydrothermal deposit samples

Sample ID	Cruise ID	Sample type	Location	Hydrothermal field	Latitude (N)	Longitude (E)	Depth (m)	Sampling device
H#893 GE1	NT08-17_leg2	stibnite agglomerate, sulfide mound	Ryukyu Arc	Wakamiko Crater, Hairy Cone vent	31°39′59″	130°46′15″	199	ROV *Hyper-Dolphin*
H#893 GE2	NT08-17_leg2	stibnite agglomerate, sulfide mound	Ryukyu Arc	Wakamiko Crater, Hairy Cone vent	31°39′59″	130°46′15″	199	ROV *Hyper-Dolphin*
H#886 GE3	NT08-17_leg1	stibnite agglomerate, sulfide mound	Ryukyu Arc	Wakamiko Crater, White Cone vent	31°40′04″	130°45′41″	191	ROV *Hyper-Dolphin*
2K1271 L1 flange, center upper	NT01-05 Leg2	active chimney flange	Okinawa Trough	Daiyon-Yonaguni Knoll	24°50'59"	122°41'57"	1364	submersible *Shinkai 2000*
2K1271 L1 flange, outer bottom, Stb	NT01-05 Leg2	active chimney flange	Okinawa Trough	Daiyon-Yonaguni Knoll	24°50'59"	122°41'57"	1364	submersible *Shinkai 2000*
2K1271 L1 flange, outer top	NT01-05 Leg2	active chimney flange	Okinawa Trough	Daiyon-Yonaguni Knoll	24°50'59"	122°41'57"	1364	submersible *Shinkai 2000*
2K1271 L1 lower outer	NT01-05 Leg2	active chimney	Okinawa Trough	Daiyon-Yonaguni Knoll	24°50'59"	122°41'57"	1364	submersible *Shinkai 2000*
2K1267 L1	NT01-05 Leg2	active chimney	Okinawa Trough	Daiyon-Yonaguni Knoll	24°50'56"	122°42'01"	1366	submersible *Shinkai 2000*
HPD#1761-R09	NT14-22	chimney	Ryukyu Arc	Daisan-Kume Knoll	26°17'20"	126°28'23"	1105	ROV *Hyper-Dolphin*

TABLE 2. Vent fluid samples (Wakamiko Crater, Ryukyu Arc)

Sample ID	Cruise ID	Location	Vent name	Type of venting fluid	Latitude (N)	Longitude (E)	Depth (m)	Temperature (°C)	*pH*	Sampling device
687R1	NT07-09	Ryukyu Arc	White Cone	focused discharge	31°40′04″	130°45′40″	194	177.6	5.99	multi-cylinder polycarbonate sample bottles with a rotary switching valve system with an all-titanium sample inlet
687R3	NT07-09	Ryukyu Arc	White Cone	focused discharge	31°40′04″	130°45′40″	194	187.0	5.86	multi-cylinder polycarbonate sample bottles with a rotary switching valve system with an all-titanium sample inlet

TABLE 3. XRD data for studied samples (Wakamiko Crater, Ryukyu Arc)

H#893 GE1		H#893 GE2		H#886 GE3		
d (Å)	*I* (%)	*d* (Å)	*I* (%)	*d* (Å)	*I* (%)	Minerals
7.9058	5	7.9921	5	7.9674	7	Sbn[a]
5.6263	49	5.6648	49	5.6554	83	Sbn
5.0270	57	5.0587	55	5.0526	76	Sbn
3.9696	21	3.9890	19	3.9857	23	Sbn
3.6235	6	3.6359	8	3.6310	6	Sbn
3.5629	100	3.5775	100	3.5754	100	Sbn
				3.5551	33	Sbn
3.4476	5	3.4581	6	3.4588	6	Sbn
3.1692	4	3.1787	4	3.1788	4	Sbn
3.1211	31	3.1316	30	3.1314	37	Sbn
3.0434	29	3.0538	30	3.0522	28	Sbn
2.7580	29	2.7669	32	2.7666	30	Sbn
2.6742	12	2.6826	12	2.6822	12	Sbn
2.6016	7	2.6101	7	2.6083	6	Sbn
2.5202	52	2.5279	49	2.5259	65	Sbn
2.4226	7	2.4279	6	2.4262	7	Sbn
2.2737	10	2.2763	11	2.2782	10	Sbn
2.2509	9	2.2538	8	2.2562	10	Sbn
2.2272	15	2.2299	13	2.2321	16	Sbn
2.0954	31	2.0999	30	2.0997	36	Sbn
1.9895	5	1.9937	5	1.9933	6	Sbn
1.9388	32	1.9426	28	1.9422	31	Sbn
1.9273	8	1.9311	8	1.9307	8	Sbn
1.9171	9	1.9208	11	1.9204	11	Sbn
1.8829	7	1.8871	7	1.8861	13	Sbn
1.8570	4	1.8614	3	1.8601	5	Sbn
1.8429	4	1.8477	3	1.8458	4	Sbn
1.7872	3	1.7894	2	1.7883	3	Sbn
1.7259	14	1.7295	12	1.7282	13	Sbn
1.6901	29	1.6928	31	1.6926	26	Sbn
1.5600	4	1.5627	2	1.5629	3	Sbn
1.5424	7	1.5444	5	1.5439	7	Sbn
1.5269	9	1.5294	8	1.5284	6	Sbn
1.4826	6	1.4846	3	1.4843	7	Sbn
1.4428	7	1.4450	5	1.4442	8	Sbn
1.4139	3	1.4160	2	1.4160	3	Sbn
1.4008	7	1.4033	5	1.4033	7	Sbn
1.3108	7	1.3120	6	1.3113	6	Sbn
1.2908	3	1.2921	3	1.2920	4	Sbn

[a] Sbn = stibnite (Warr 2021): data from Kyono and Kimata (2004).

TABLE 4. Mineralogy (XRD) of the samples (Wakamiko Crater, Ryukyu Arc)

Sample ID	Mineralogy
H#893 GE1	stibnite, metastibnite, talc-smectite (?)
H#893 GE2	stibnite, metastibnite, talc-smectite (?)
H#886 GE3	stibnite, metastibnite, talc-smectite (?)

TABLE 5. Orthorhombic unit-cell parameters of stibnite (Wakamiko Crater, Ryukyu Arc)

Sample ID	*a* (Å)	*b* (Å)	*c* (Å)
H#893 GE1	11.2115(5)	11.2940(4)	3.8317(3)
H#893 GE2	11.2393(5)	11.3174(4)	3.8385(3)
H#886 GE3	11.2349(5)	11.3161(4)	3.8336(2)

TABLE 6. Mineral chemistry (EMP data) and empirical formulae of stibnite (Wakamiko Crater, Ryukyu Arc)

Sample ID	#[a]	S (wt.%)	Sn	Sb	Pb	Zn	Fe	Cu	As	Total	S (at.%)	Sn	Sb	Pb	Zn	Fe	Cu	As	Total	Empirical formulae
H#893 GE1	7	27.50	0.43	69.96	0.06	0.12	0.11	0.14	0.39	98.71	59.39	0.25	39.80	0.01	0.06	0.07	0.04	0.36	100.00	$(Sb_{1.99}As_{0.02}Sn_{0.01})S_{2.97}$
H#893 GE2	14	27.81	0.47	70.29	0.07	0.12	0.05	0.08	0.20	99.09	59.66	0.27	39.72	0.02	0.07	0.03	0.04	0.18	100.00	$(Sb_{1.99}As_{0.01}Sn_{0.01})S_{2.98}$
H#886 GE3	7	28.00	0.43	70.05	0.07	0.09	0.07	0.10	0.14	98.95	59.99	0.25	39.53	0.02	0.03	0.02	0.02	0.13	100.00	$(Sb_{1.98}As_{0.01}Sn_{0.01})S_{3.00}$
detection limits (ppm)		78	160	165	144	161	95	131	156											

[a] Number of EMP analyses.

TABLE 7. Chemical (ICP-OES) and S isotope compositions of the hydrothermal deposits (Wakamiko Crater, Ryukyu Arc)

Sample ID	Al (ppm)	Ca	Cd	Co	Cr	Cu	Fe	K	Li	Mg	Mn	Mo	Na	Ni	P	Pb	Sr	V	Zn	Sb	$(\delta^{34}S_{sulfide})^a$ (‰)
H#893 GE1	8069	b.d.l.[b]	b.d.l.	b.d.l.	b.d.l.	b.d.l.	2385	1359	75.5	46561	b.d.l.	b.d.l.	5297	b.d.l.	b.d.l.	b.d.l.	b.d.l.	b.d.l.	b.d.l.	541274	3.6
H#893 GE2	10834	b.d.l.	148	b.d.l.	b.d.l.	b.d.l.	6928	b.d.l.	b.d.l.	13541	b.d.l.	b.d.l.	b.d.l.	b.d.l.	b.d.l.	b.d.l.	51.3	40.1	b.d.l.	610371	3.2
H#886 GE3	2939	b.d.l.	b.d.l.	b.d.l.	b.d.l.	b.d.l.	2696	b.d.l.	b.d.l.	5912	b.d.l.	b.d.l.	1110	b.d.l.	b.d.l.	b.d.l.	b.d.l.	b.d.l.	97.1	559576	2.8
Standards																					
Nod-P-1 (measured)	27100	21977	b.d.l.	2299	b.d.l.	11887	59452	9763	141	20923	304094	616	17081	13752	2180	711	644	637	1721		
Nod-P-1 (reference)[c]	25400	22160	22.6	2240	13.3	11500	58050	9960	140	19900	291300	760	16300	13400	2010	560	680	570	1600		
Nod-A-1 (measured)	22512	112062	b.d.l.	3184	b.d.l.	1087	111631	4724	72.6	30234	188632	364	8199	6449	5476	1054	1524	691	627		
Nod-A-1 (reference)[c]	20480	110100	7.5	3110	20.9	1110	109100	4981	76.1	28700	185000	390	7420	6360	5920	846	1630	660	590		
Detection limits (ppm)	1699	1123	48.4	68.2	62.9	76.6	1236	1279	66.0	480	262	213	1006	93.0	1100	407	50.2	38.6	49.8	954	

[a] Averages of two duplicate measurements.
[b] b.d.l. = below detection limits.
[c] Axelsson et al. (2002).

TABLE 8. Chemical (ICP-MS) and S isotope compositions of the vent fluids (Wakamiko Crater, Ryukyu Arc)

Sample ID	Vent name	T_{max}[a] (°C)	*pH*[a]	Alkalinity[a] (meq/L)	Si[a] (mmol/kg)	H_2S[a]	Cl[a]	SO_4^{2-}[a]	Mg[a]	Ca[a]	Na[a]	K[a]	Fe (nmol/kg)	Mn	Zn	Pb	Cu	Ni	Mo	Sb	V	Co
687R1	White Cone	177.6	5.99	8.50	5.20	0.14	340	6.3	10.5	4.9	278	16.5	1839	69.0	45.4	0.13	b.d.l.[b]	34.0	34.8	84.6	18.0	0.32
687R3	White Cone	187.0	5.86	9.50	5.26	0.17	321	5.9	10	4.8	275	16.4	427	75.7	17.6	0.16	b.d.l.	8.22	30.6	220	10.9	0.39
Standard																						
CASS-6 (measured)		-	-	-	n.m.[c]	n.m.	n.m.	n.m.	n.m.	n.m.	n.m.	n.m.	52.6	19.5	22.4	0.13	10.6	7.21	110	n.m.	9.08	1.32
CASS-6 (reference)		-	-	-	-	-	-	-	-	-	-	-	27.4	39.7	19.0	0.05	8.18	6.99	93.4	-	9.62	1.12

[a] Data from Yamanaka et al. (2013).
[b] b.d.l. = below detection limits.
[c] n.m. = not measured.

Sample ID	Vent name	Cd (nmol/kg)	U	Y	La	Ce	Pr	Nd	Sm	Eu	Gd	Tb	Dy	Ho	Er	Tm	Yb	Lu	ΣREE (ppb)	(Ce/Ce*)[d]	(Eu/Eu*)[e]	($\delta^{34}S_{sulfate}$)[f] (‰)
687R1	White Cone	0.08	2.68	0.03	0.021	0.078	b.d.l.	0.014	b.d.l.	0.080	b.d.l.	b.d.l.	b.d.l.	b.d.l.	b.d.l.	b.d.l.	b.d.l.	b.d.l.	0.03	2.88	-	22.0
687R3	White Cone	0.07	1.34	0.03	0.031	0.058	b.d.l.	0.019	b.d.l.	0.124	0.007	b.d.l.	b.d.l.	b.d.l.	b.d.l.	b.d.l.	b.d.l.	b.d.l.	0.04	1.45	113	21.6
Standard																						
CASS-6 (measured)		0.41	10.3	0.23	0.086	0.050	0.012	0.060	0.013	0.002	0.015	b.d.l.	0.011	0.002	0.008	b.d.l.	0.009	0.002	0.04	0.34	0.51	-
CASS-6 (reference)		0.19	12.0	-	-	-	-	-	-	-	-	-	-	-	-	-	-	-	-	-	-	-

[d] $Ce/Ce^* = 2Ce_{CN}/(La_{CN}+Nd_{CN})$; CN = chondrite-normalized (McDonough and Sun 1995).
[e] $Eu/Eu^* = 2Eu_{CN}/(Nd_{CN}+Gd_{CN})$.
[f] Averages of two duplicate measurements.

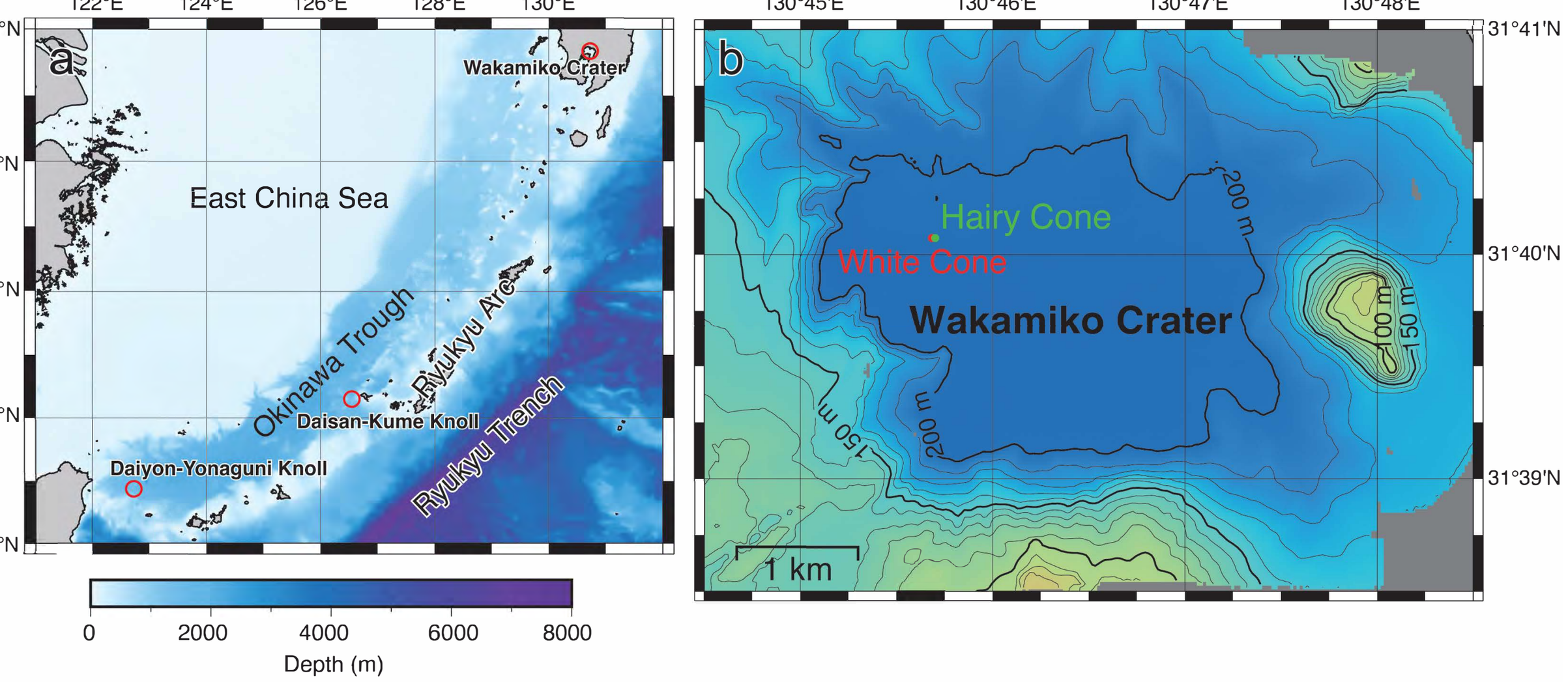
a
b
Wakamiko Crater
East China Sea
Okinawa Trough
Ryukyu Arc
Daisan-Kume Knoll
Daiyon-Yonaguni Knoll
Ryukyu Trench
Hairy Cone
White Cone
Wakamiko Crater
200 m
150 m
100 m
150 m
1 km
122°E
124°E
126°E
128°E
130°E
130°45'E
130°46'E
130°47'E
130°48'E
31°41'N
31°40'N
31°39'N
0
2000
4000
6000
8000
Depth (m)

Figure 1

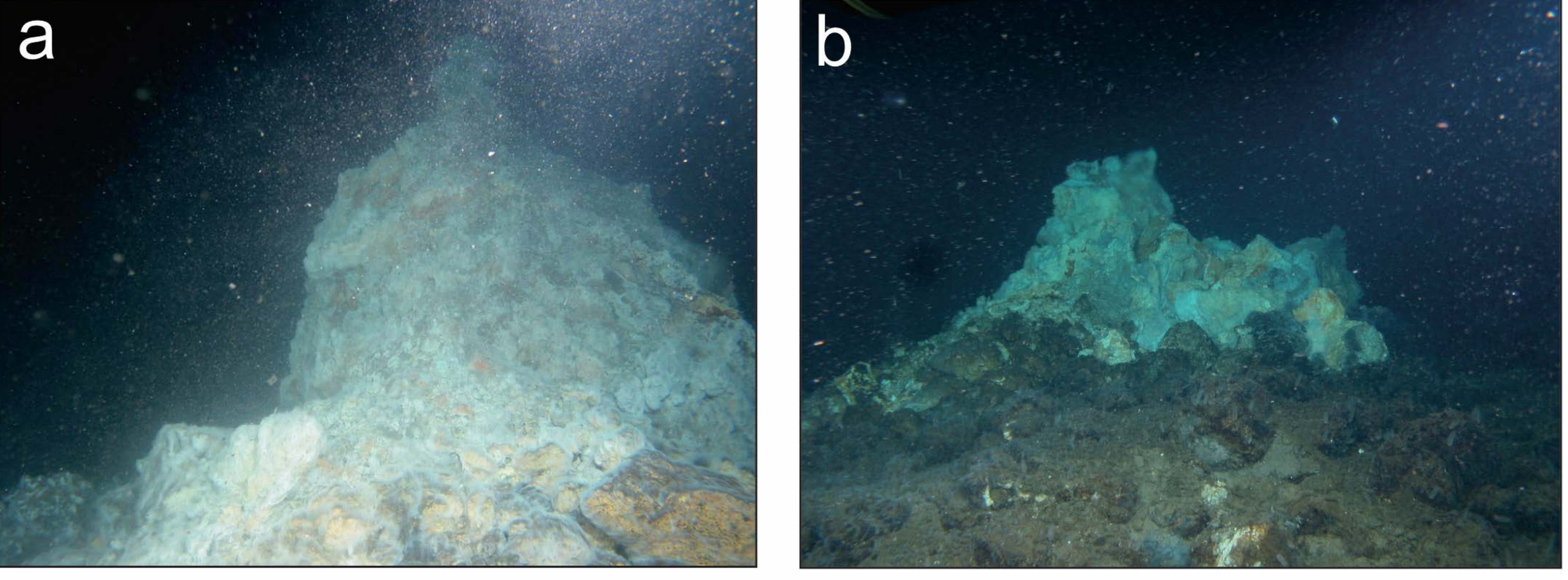

Figure 2

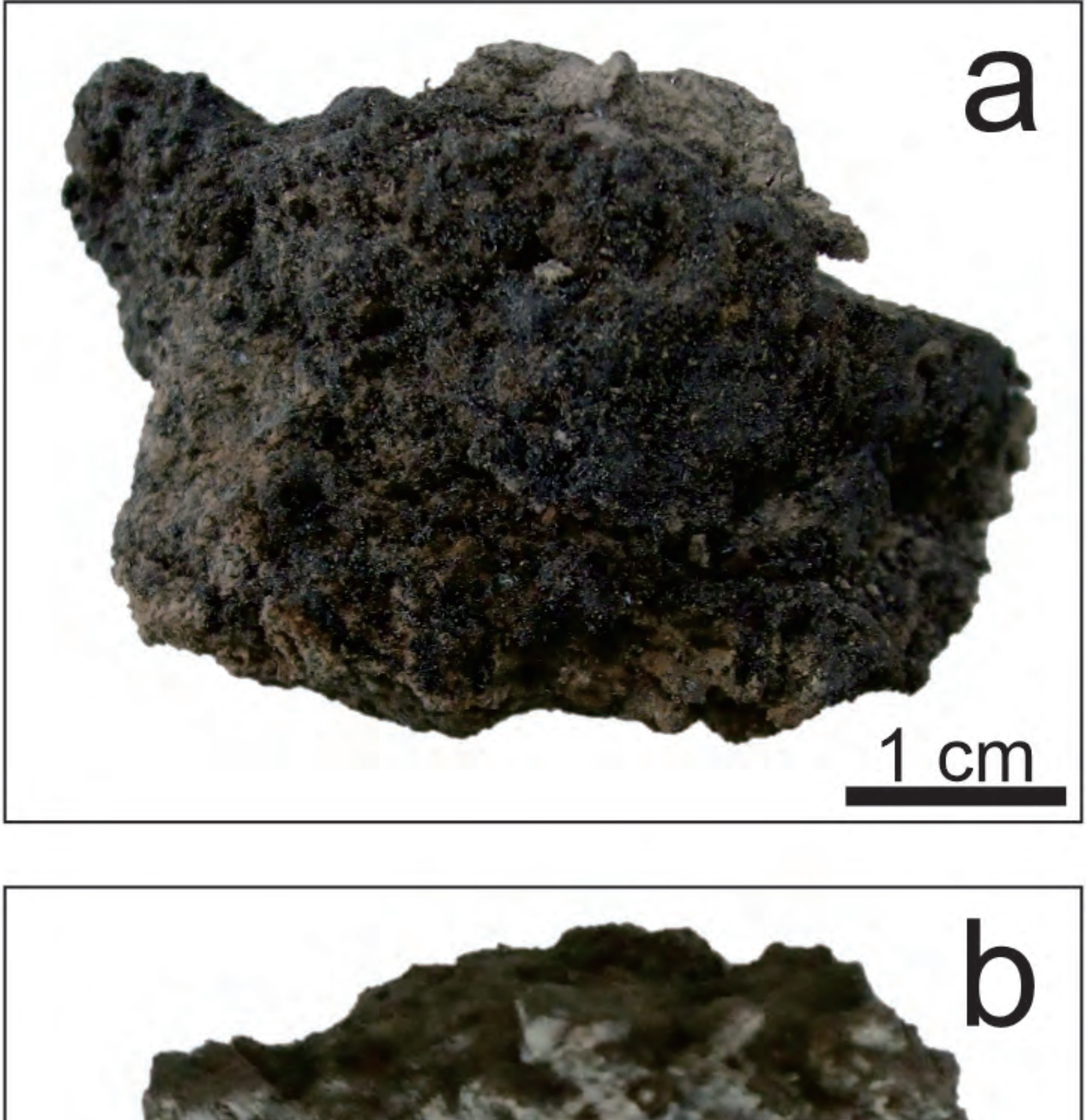

Figure 3

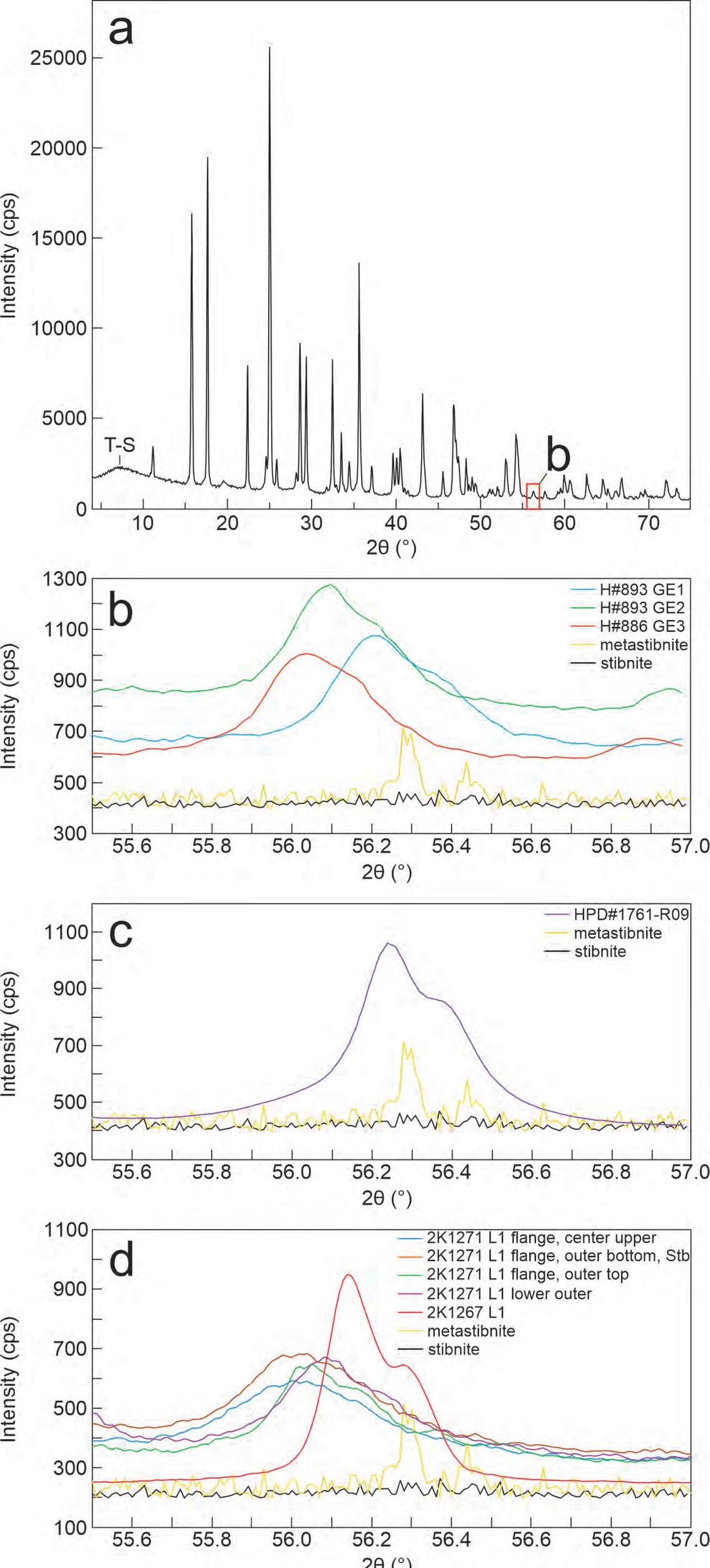
a
Intensity (cps)
25000
20000
15000
10000
5000
0
T-S
b
10
20
30
40
50
60
70
2θ (°)
b
Intensity (cps)
1300
1100
900
700
500
300
H#893 GE1
H#893 GE2
H#886 GE3
metastibnite
stibnite
55.6
55.8
56.0
56.2
56.4
56.6
56.8
57.0
2θ (°)
c
Intensity (cps)
1100
900
700
500
300
HPD#1761-R09
metastibnite
stibnite
55.6
55.8
56.0
56.2
56.4
56.6
56.8
57.0
2θ (°)
d
Intensity (cps)
1100
900
700
500
300
100
2K1271 L1 flange, center upper
2K1271 L1 flange, outer bottom, Stb
2K1271 L1 flange, outer top
2K1271 L1 lower outer
2K1267 L1
metastibnite
stibnite
55.6
55.8
56.0
56.2
56.4
56.6
56.8
57.0
2θ (°)

Figure 4

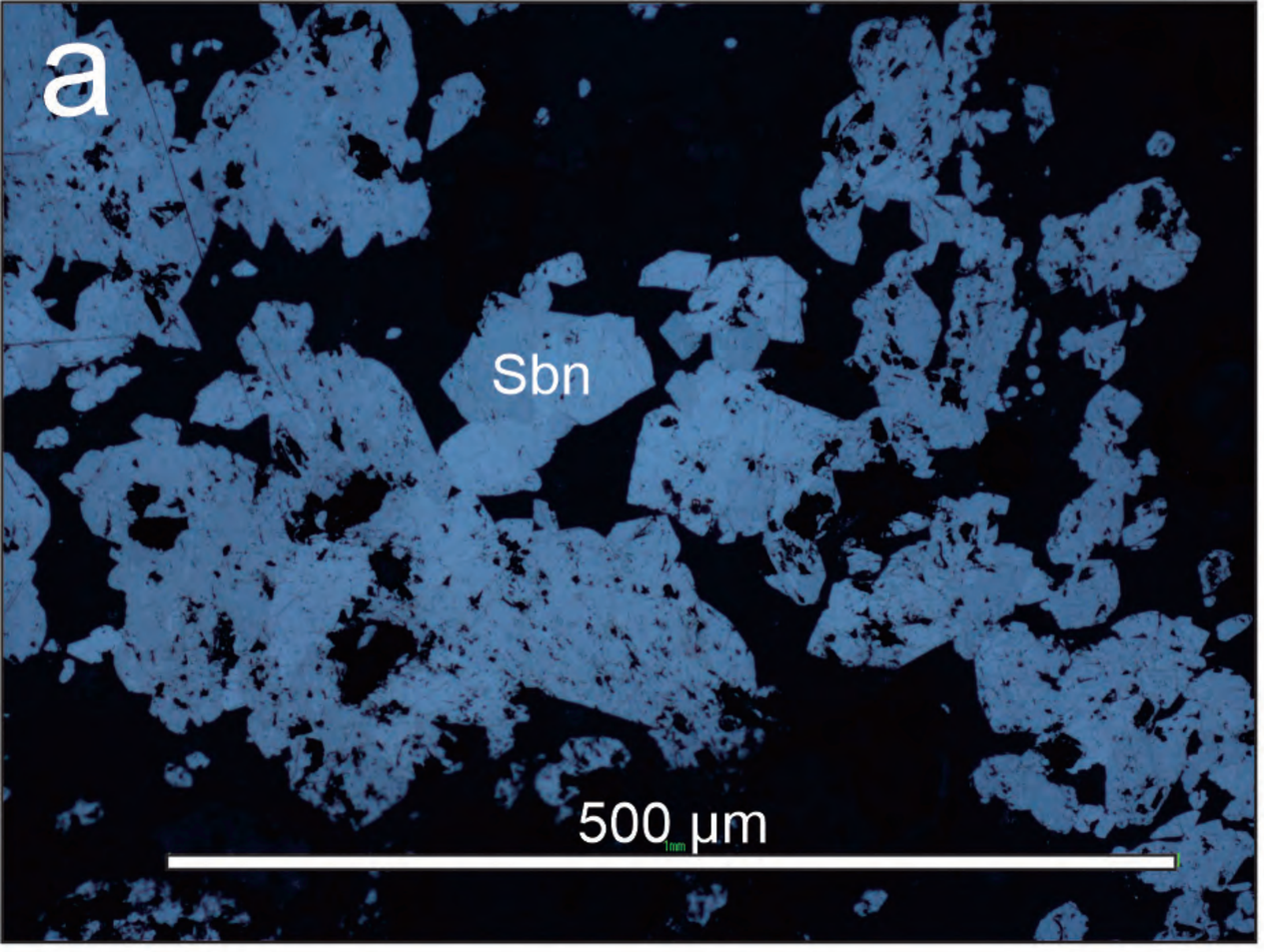
a
Sbn
500 µm

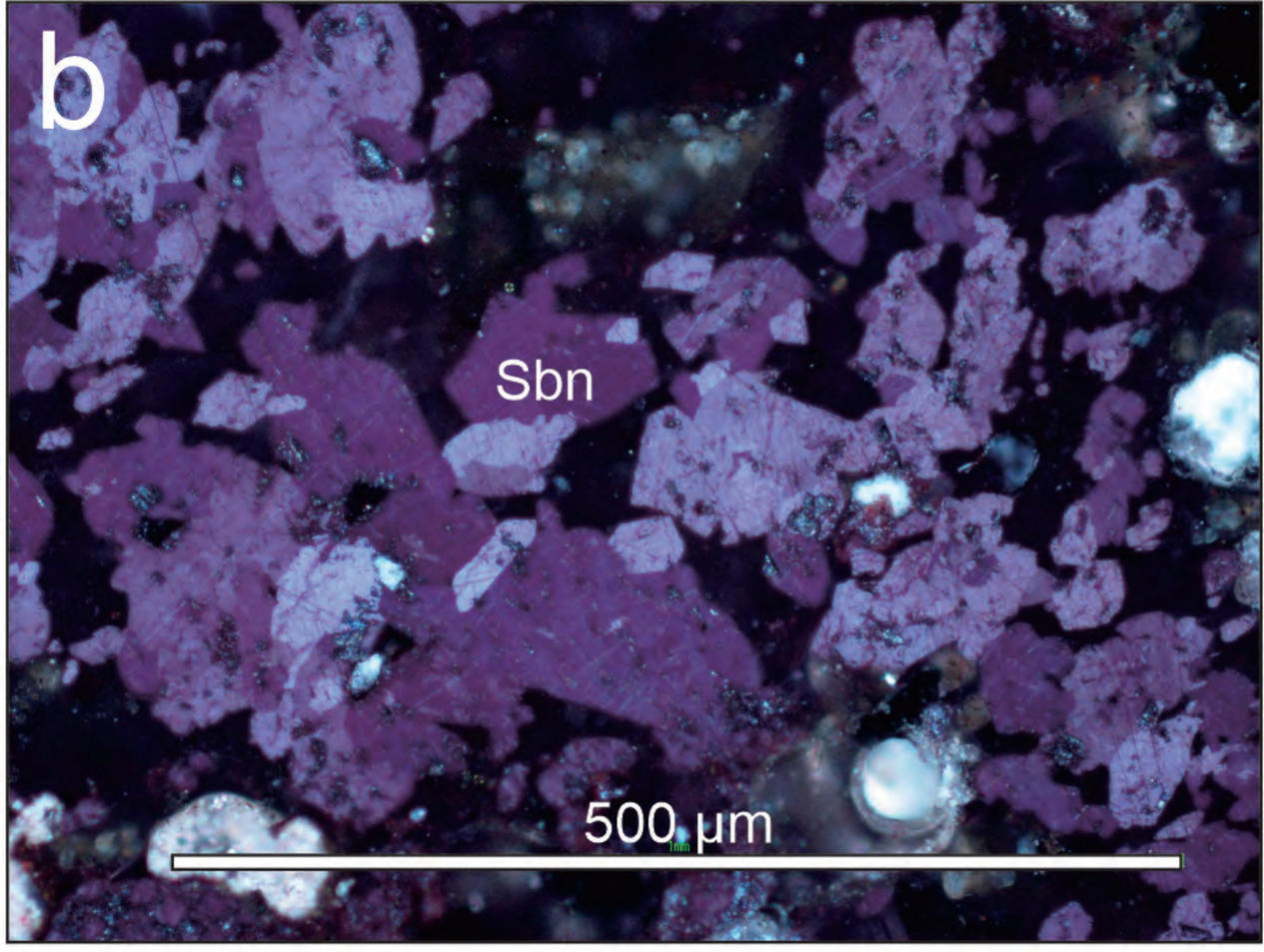
b
Sbn
500 µm

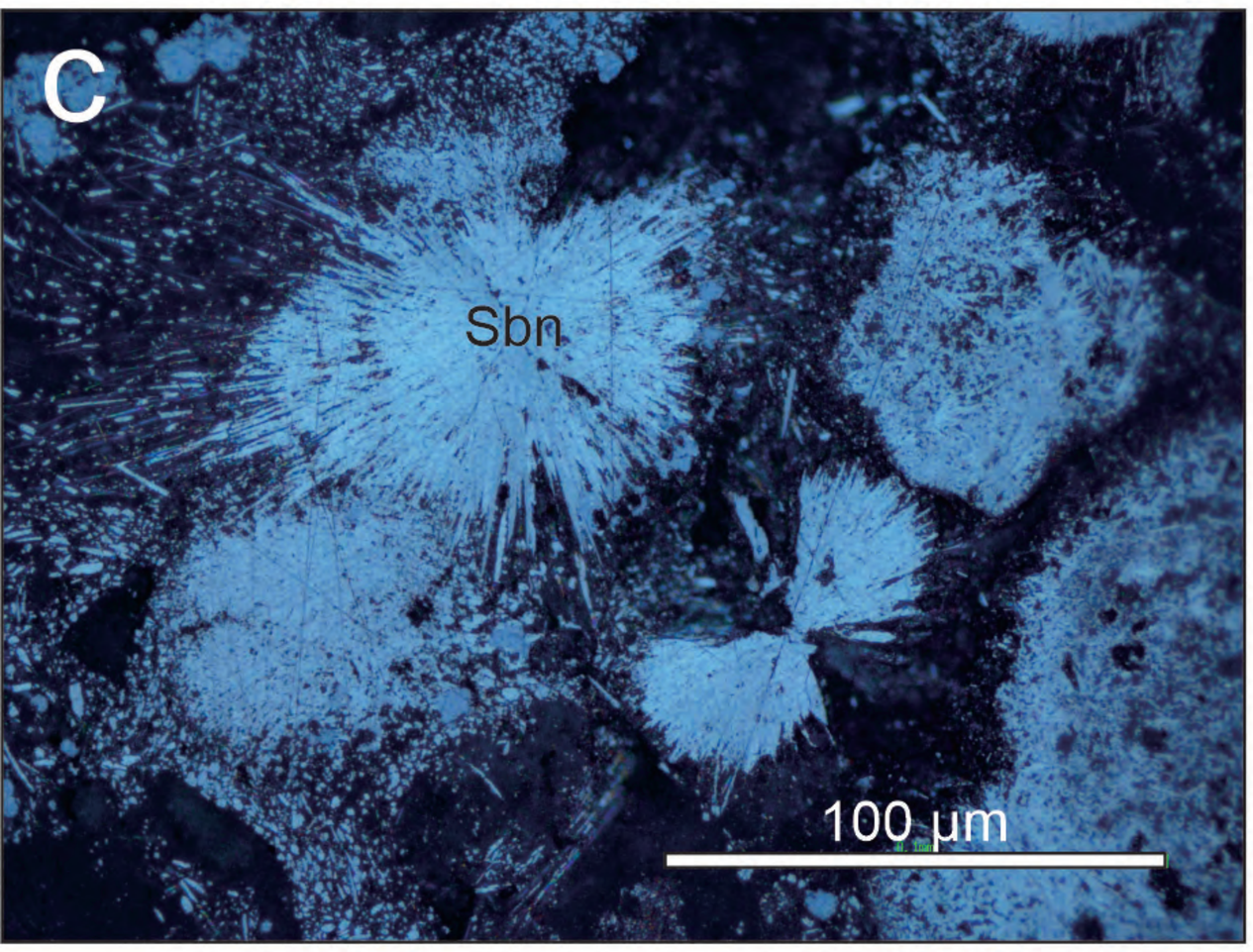
c
Sbn
100 µm

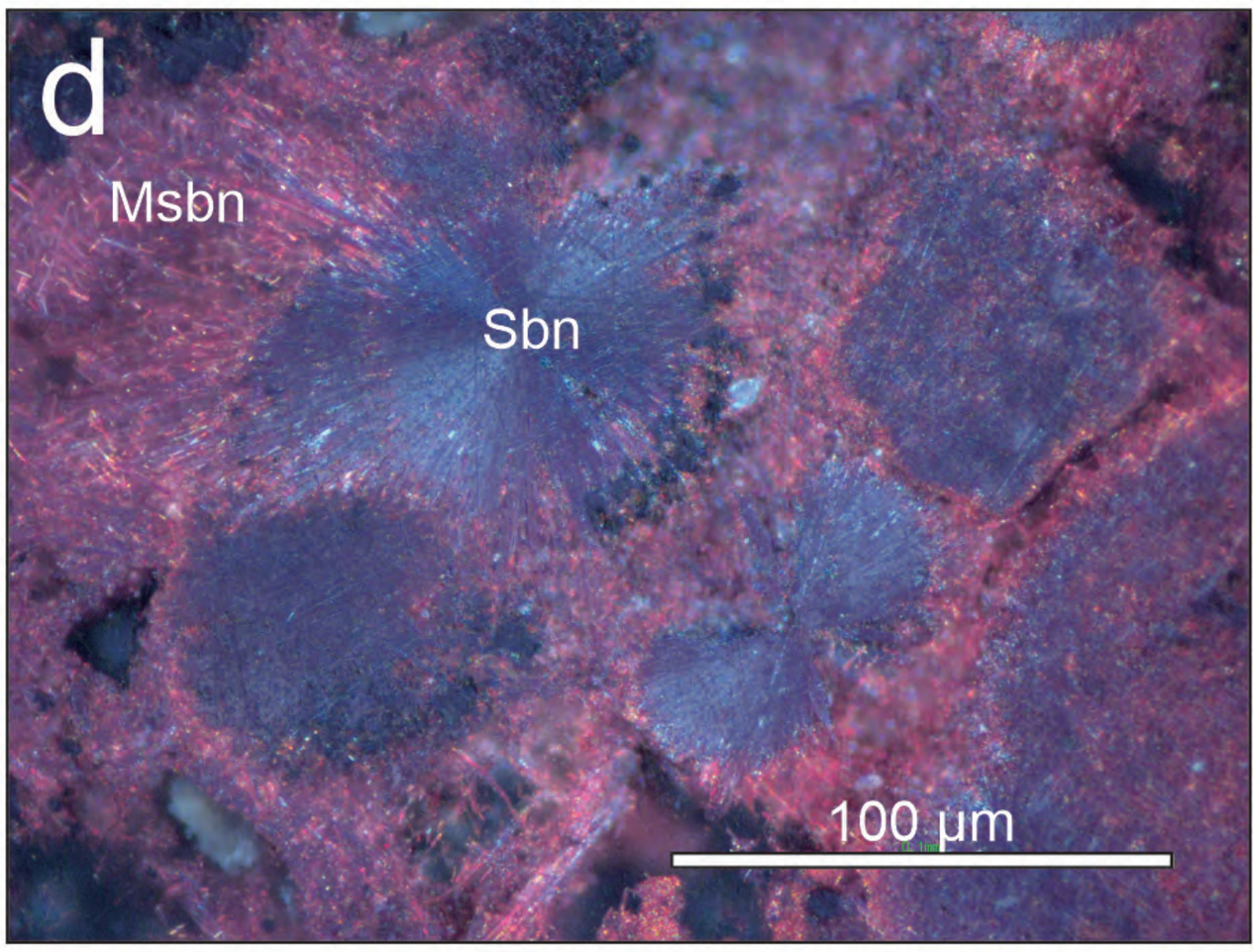
d
Msbn
Sbn
100 µm

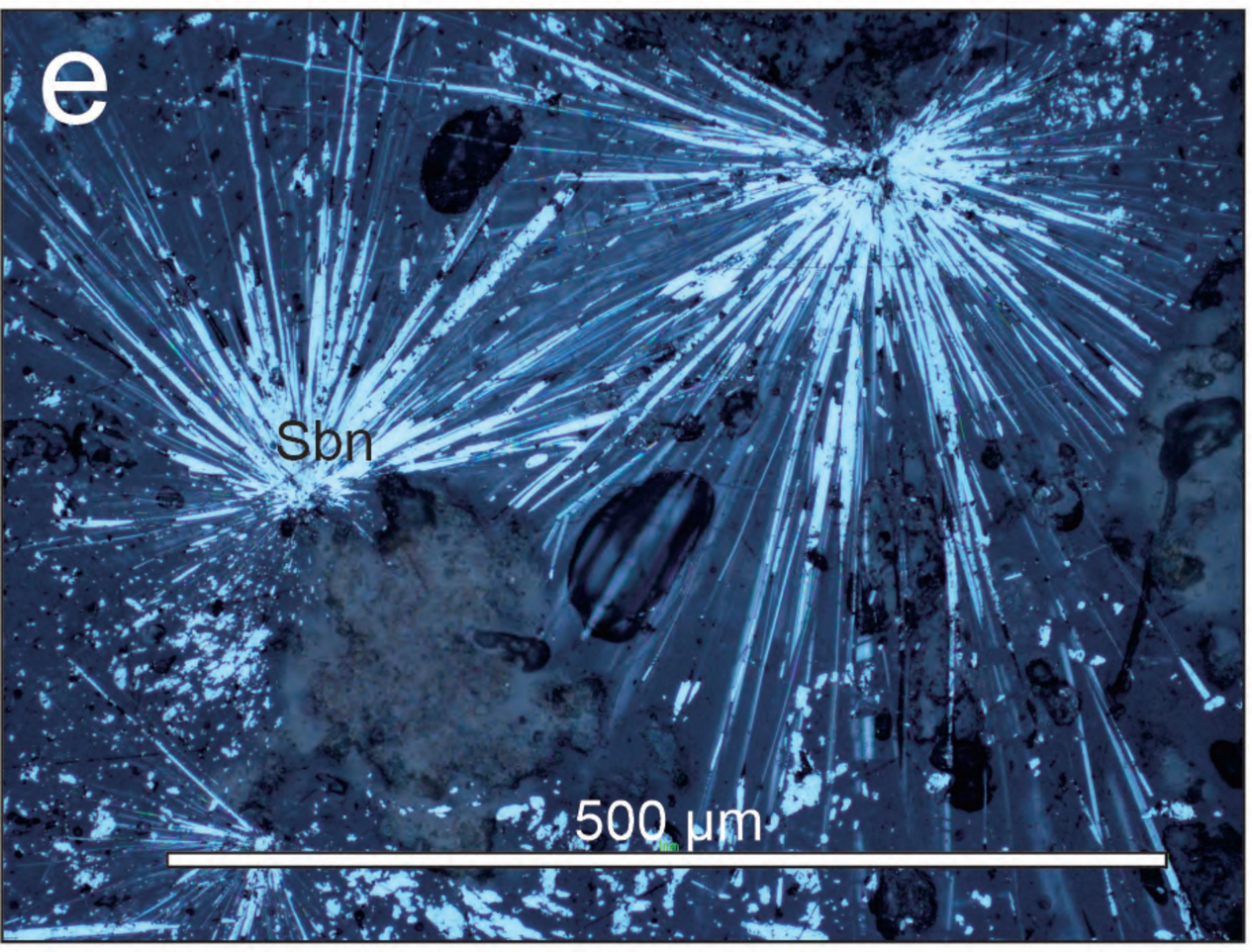
e
Sbn
500 µm

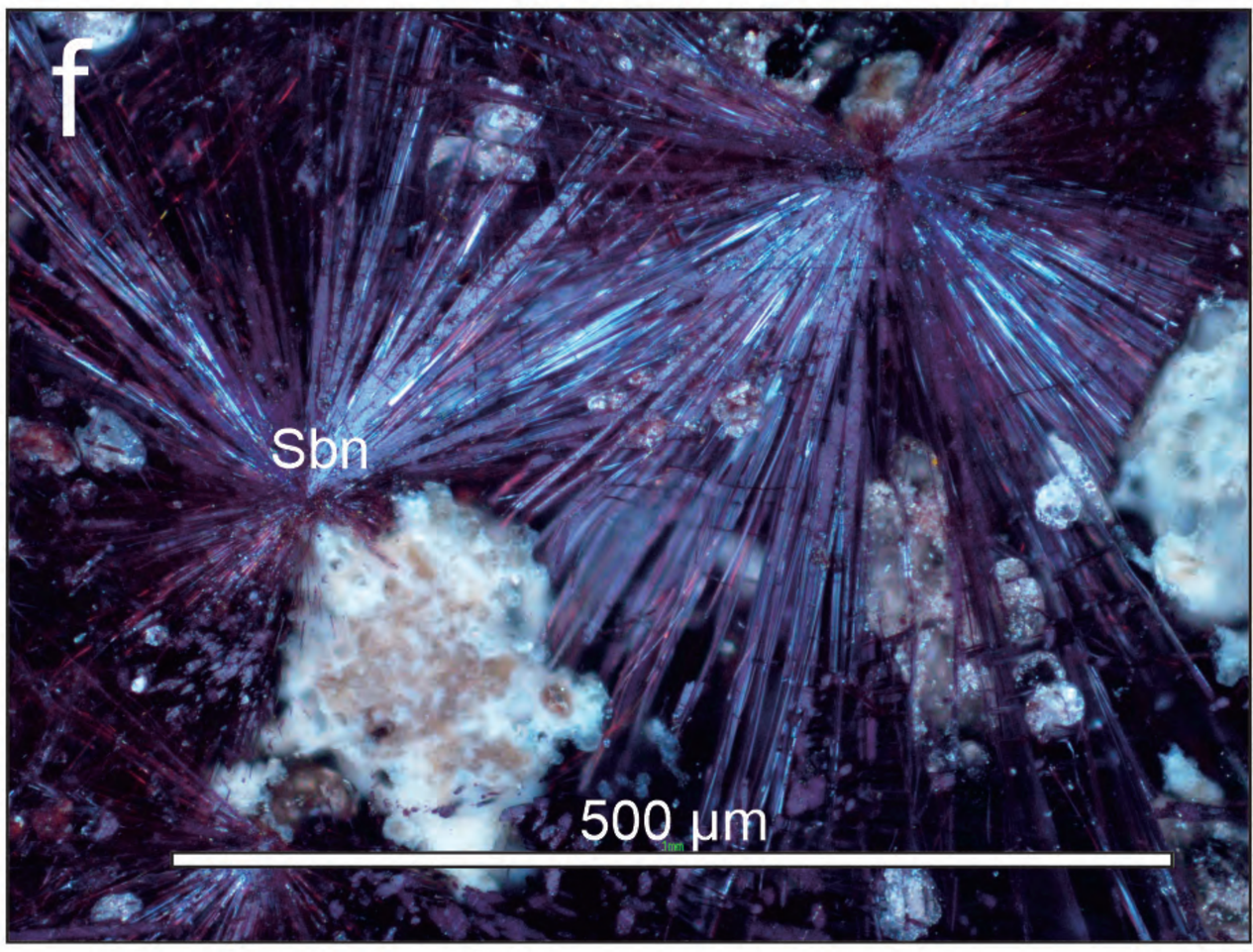
f
Sbn
500 µm

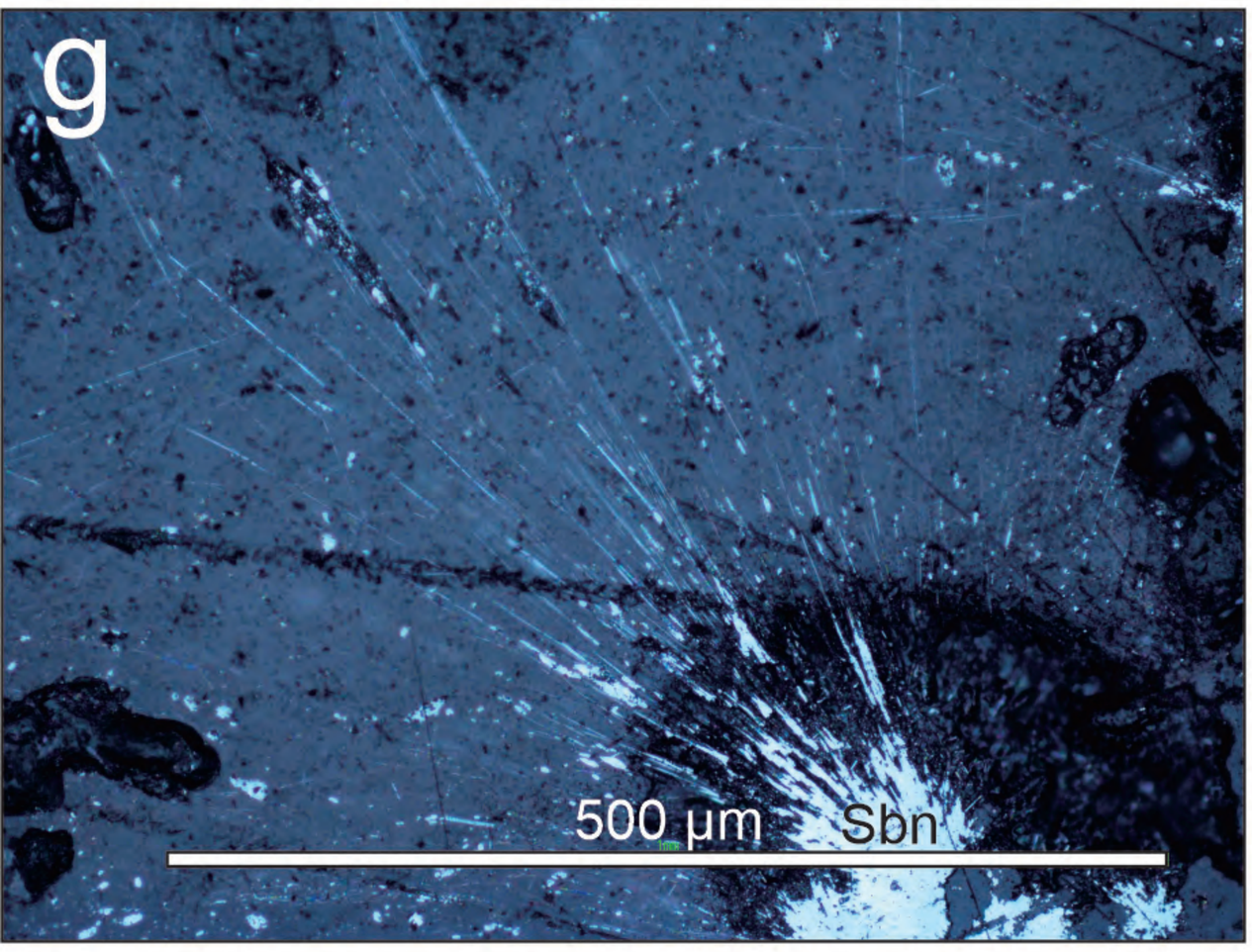
g
500 µm
Sbn

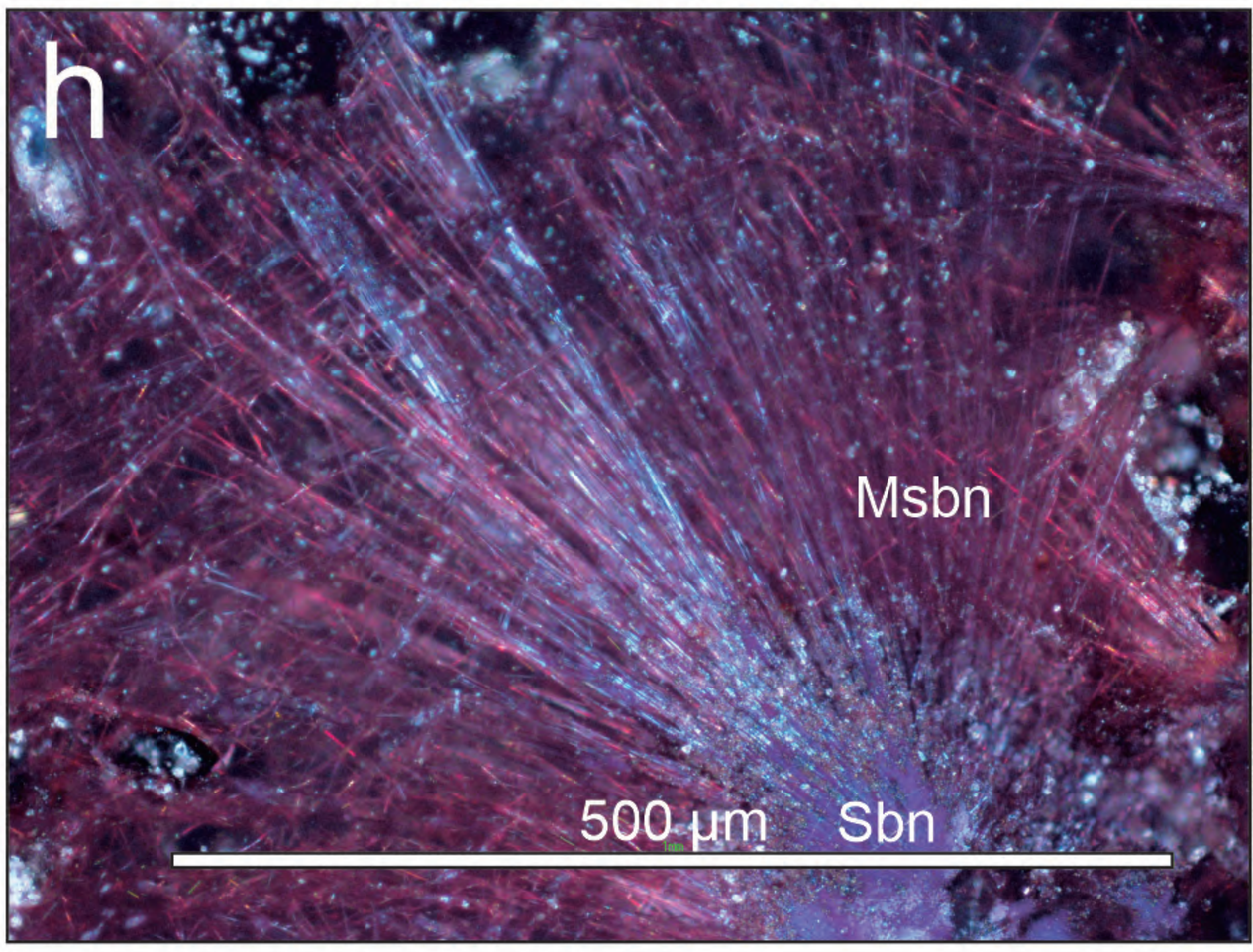
h
Msbn
500 µm
Sbn

Figure 5

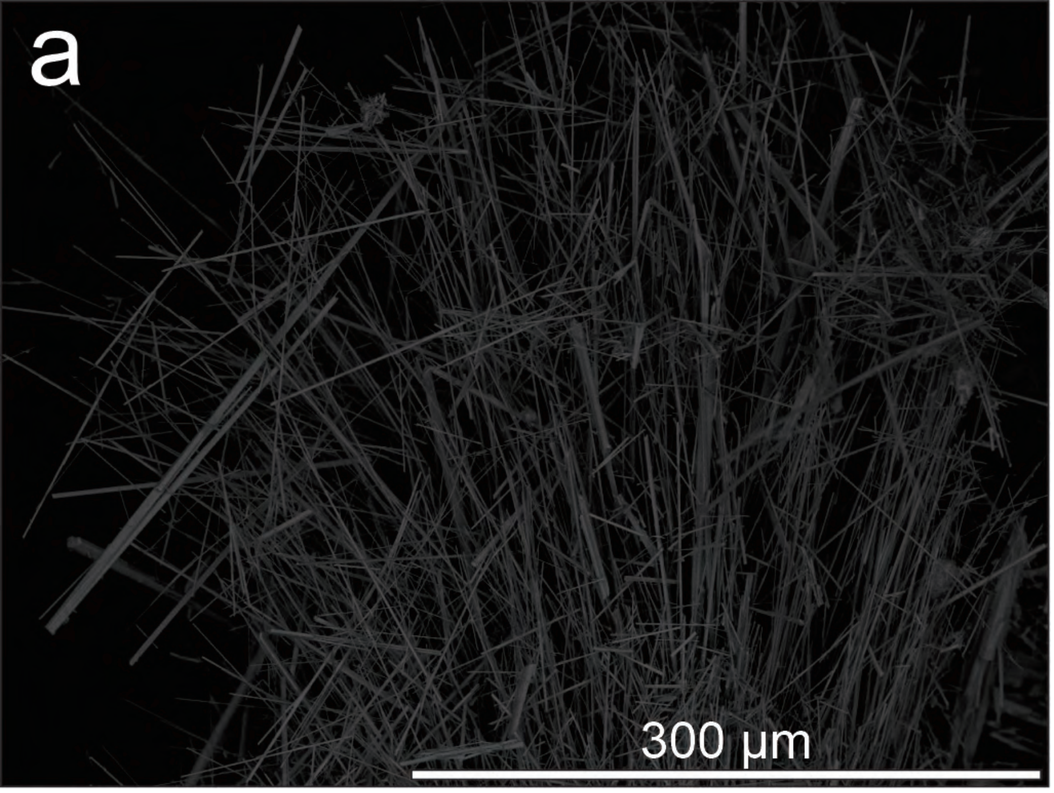

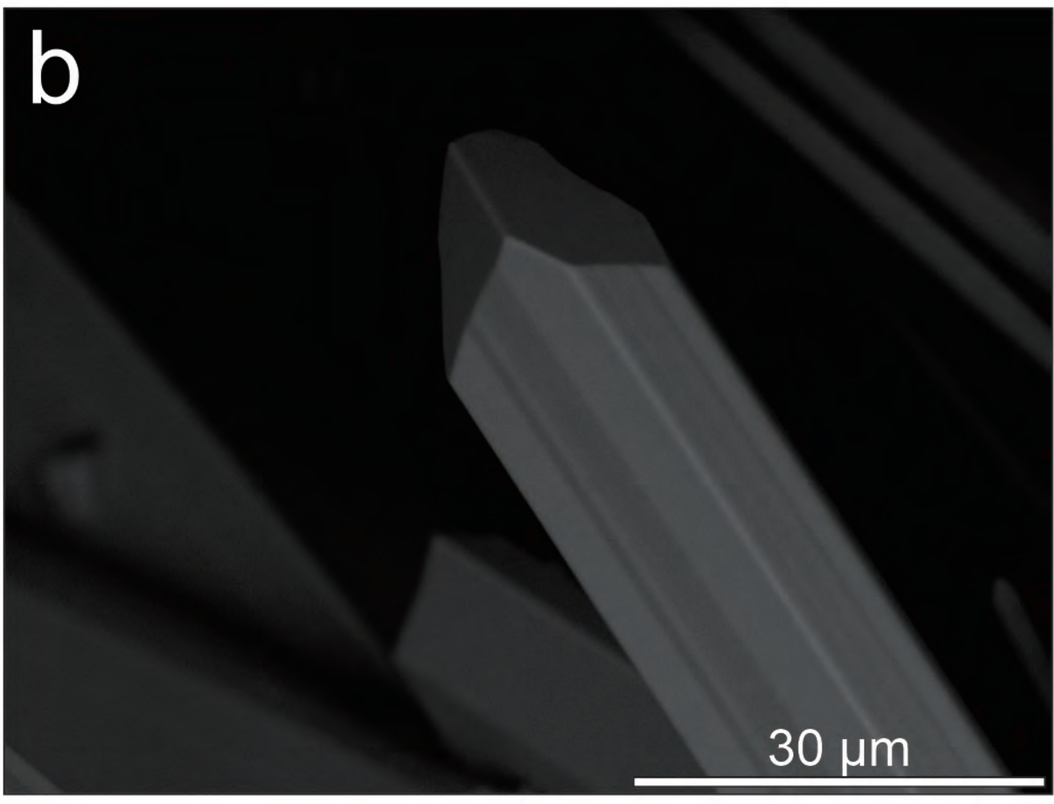

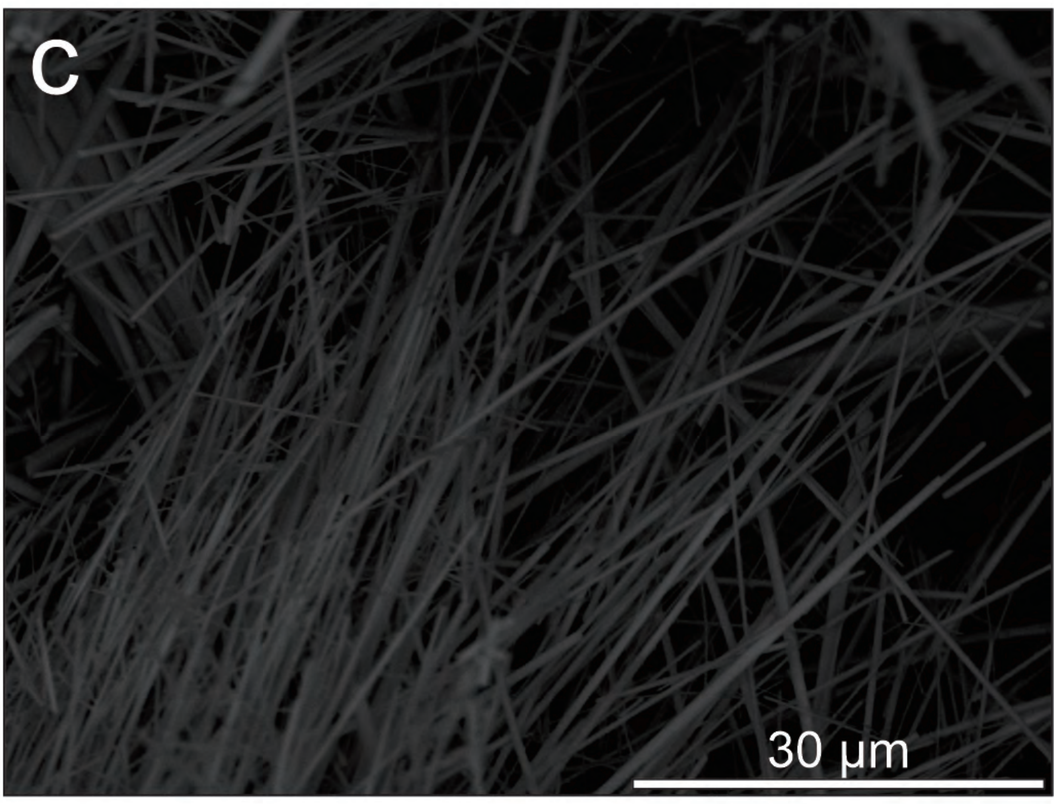

Figure 6

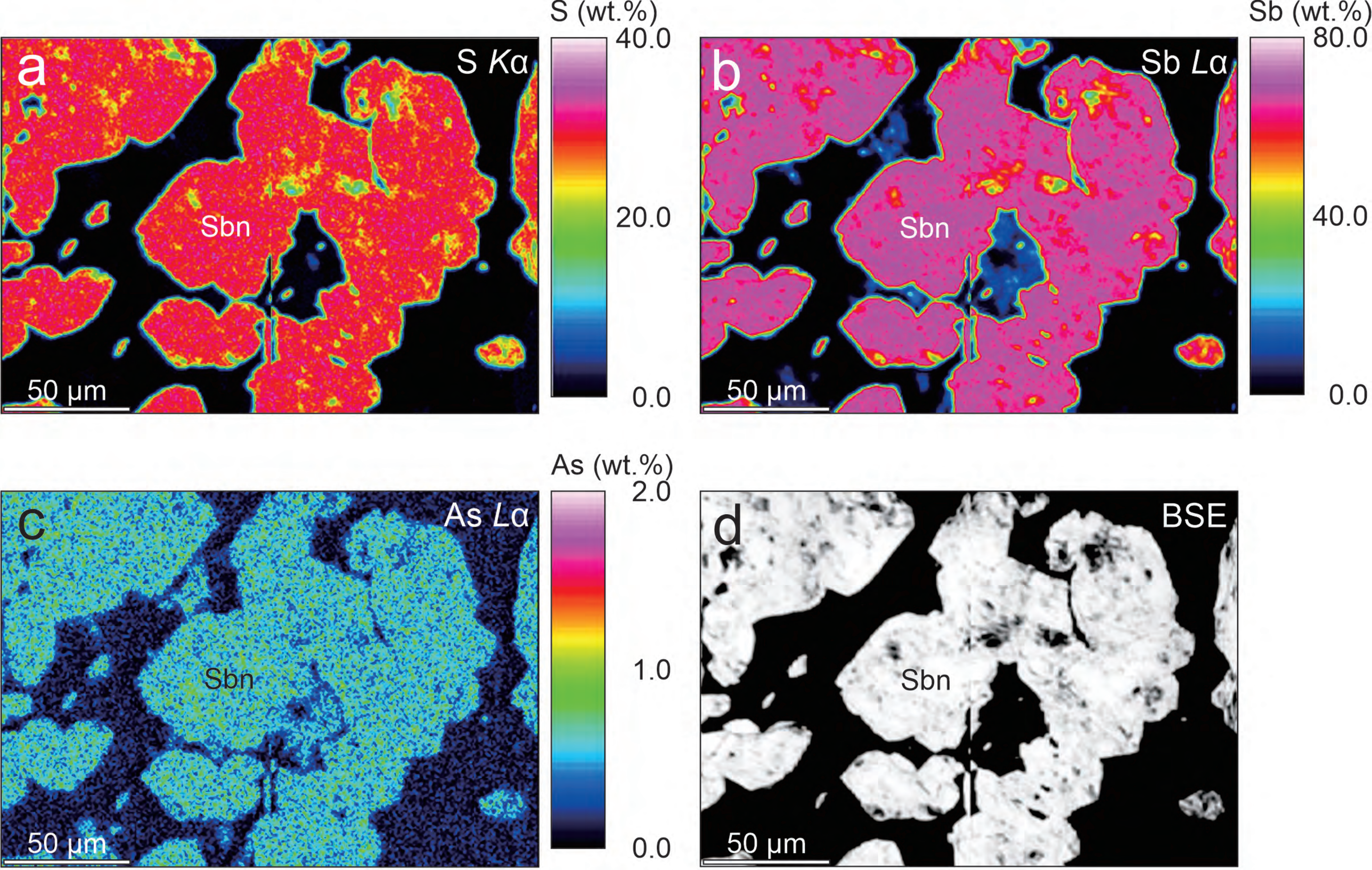
a
S Kα
Sbn
50 μm
S (wt.%)
40.0
20.0
0.0
b
Sb Lα
Sbn
50 μm
Sb (wt.%)
80.0
40.0
0.0
C
As Lα
Sbn
50 μm
As (wt.%)
2.0
1.0
0.0
d
BSE
Sbn
50 μm

Figure 7

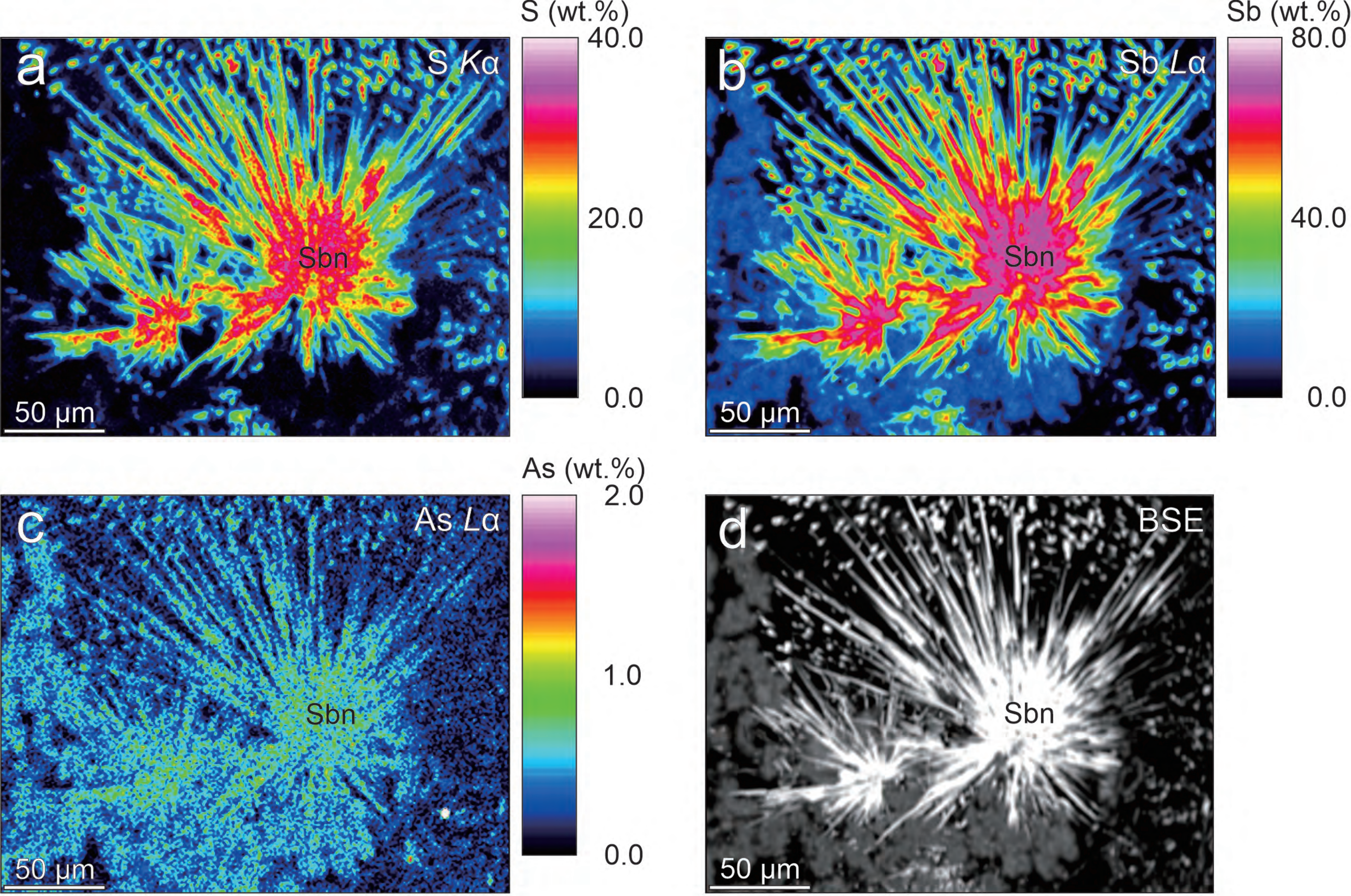
a
S Kα
Sbn
50 μm
S (wt.%)
40.0
20.0
0.0
b
Sb Lα
Sbn
50 μm
Sb (wt.%)
80.0
40.0
0.0
c
As Lα
Sbn
50 μm
As (wt.%)
2.0
1.0
0.0
d
BSE
Sbn
50 μm

Figure 8

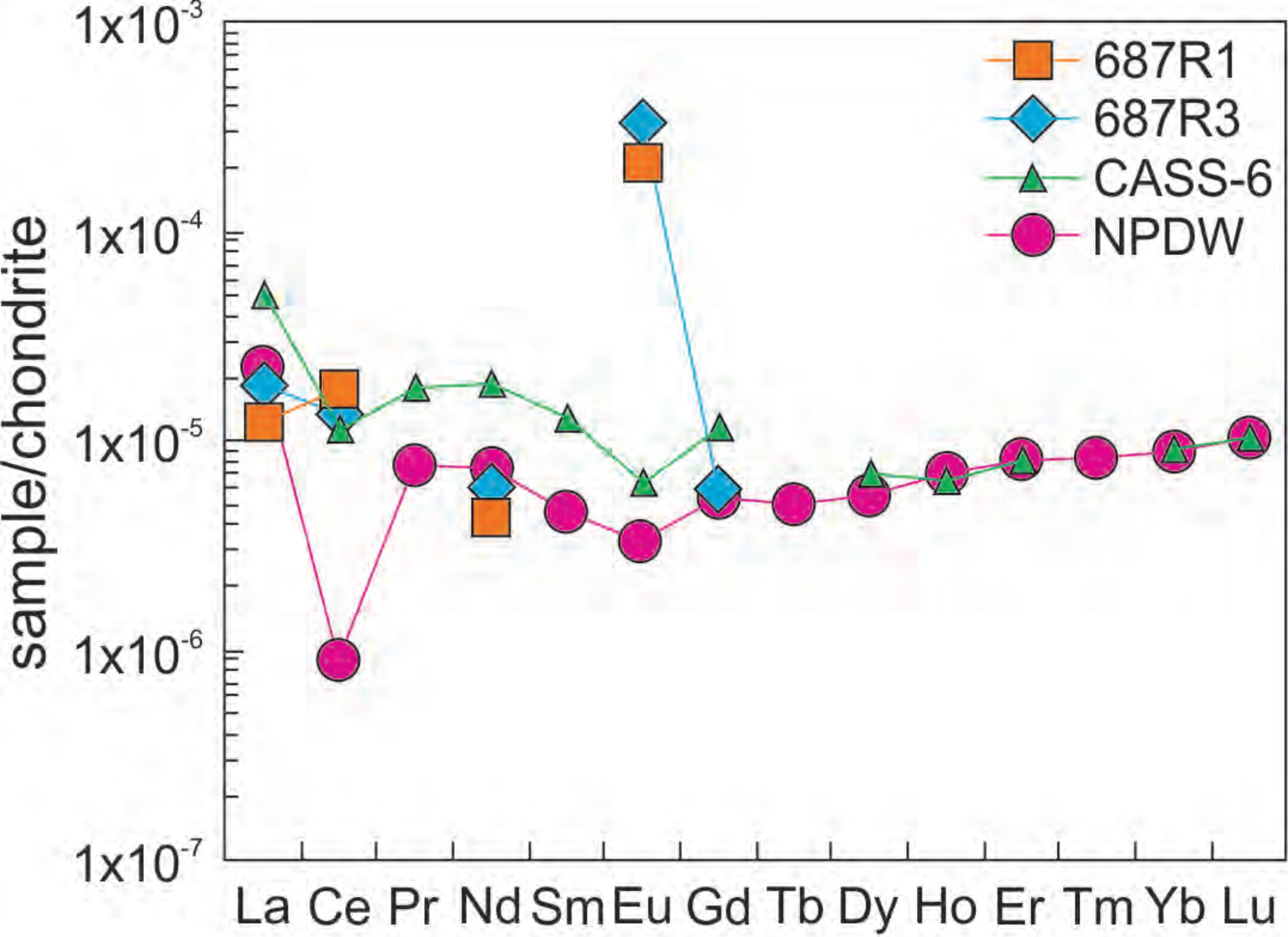
1x10-3
1x10-4
1x10-5
1x10-6
1x10-7
sample/chondrite
687R1
687R3
CASS-6
NPDW
La Ce Pr Nd Sm Eu Gd Tb Dy Ho Er Tm Yb Lu

Figure 9

a

$HSb_2S_4^-$

Stibnite

$Sb(OH)_{3(aq)}$

Sb_2O_3

177.6°C

e

$HSb_2S_4^-$

Stibnite

$Sb(OH)_{3(aq)}$

Sb_2O_3

177.6°C

i

$HSb_2S_4^-$

$Sb(OH)_{3(aq)}$

177.6°C

b

$HSb_2S_4^-$

Stibnite

$Sb(OH)_{3(aq)}$

Sb_2O_3

150°C

f

$HSb_2S_4^-$

Stibnite

$Sb(OH)_{3(aq)}$

Sb_2O_3

150°C

j

$HSb_2S_4^-$

$Sb(OH)_{3(aq)}$

100°C

c

$HSb_2S_4^-$

Stibnite

$Sb(OH)_{3(aq)}$

Sb_2O_3

100°C

g

$HSb_2S_4^-$

Stibnite

$Sb(OH)_{3(aq)}$

Sb_2O_3

100°C

k

$HSb_2S_4^-$

Stibnite

$Sb(OH)_{3(aq)}$

50°C

d

$HSb_2S_4^-$

Stibnite

$Sb(OH)_{3(aq)}$

Sb_2O_3

50°C

h

$HSb_2S_4^-$

Stibnite

$Sb(OH)_{3(aq)}$

Sb_2O_3

50°C

l

$HSb_2S_4^-$

Stibnite

Sb_2O_5

Sb

Sb_2O_4

$Sb(OH)_3$

25°C

0 -2 -4 -6 -8 -10

$\log_{10}\mathbf{a}_{[H_2S_{(aq)}]}$

-10 -8 -6 -4 -2 0

$\log_{10}\mathbf{a}_{[HSb_2S_4^-]}$

$\log_{10}\mathbf{a}_{[Sb(OH)_{3(aq)}]}$

-0.5 0.0 0.5 1.0

Eh (volts)

Figure 10

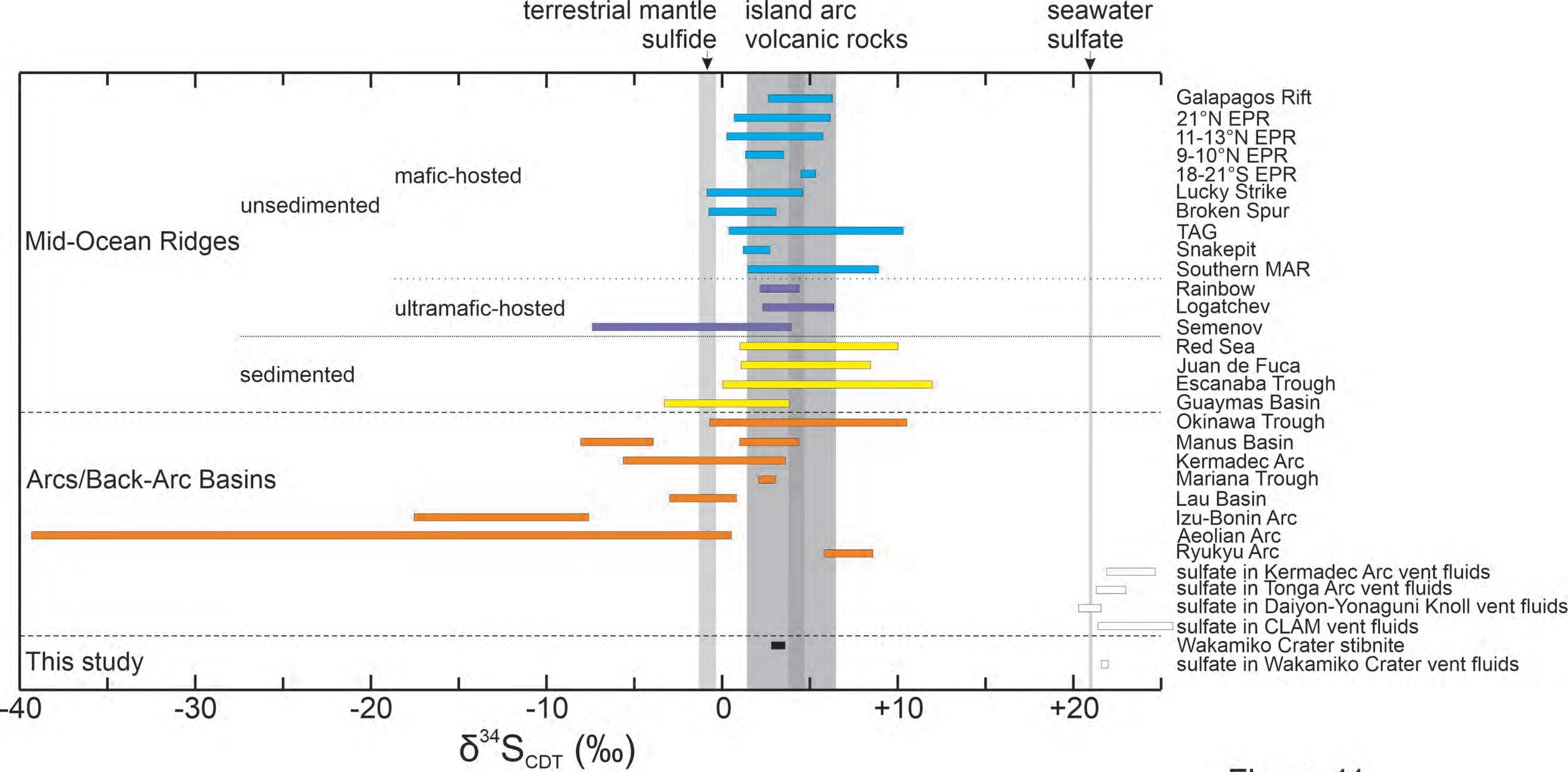
terrestrial mantle sulfide
island arc volcanic rocks
seawater sulfate
mafic-hosted
unsedimented
Mid-Ocean Ridges
ultramafic-hosted
sedimented
Arcs/Back-Arc Basins
This study
Galapagos Rift
21°N EPR
11-13°N EPR
9-10°N EPR
18-21°S EPR
Lucky Strike
Broken Spur
TAG
Snakepit
Southern MAR
Rainbow
Logatchev
Semenov
Red Sea
Juan de Fuca
Escanaba Trough
Guaymas Basin
Okinawa Trough
Manus Basin
Kermadec Arc
Mariana Trough
Lau Basin
Izu-Bonin Arc
Aeolian Arc
Ryukyu Arc
sulfate in Kermadec Arc vent fluids
sulfate in Tonga Arc vent fluids
sulfate in Daiyon-Yonaguni Knoll vent fluids
sulfate in CLAM vent fluids
Wakamiko Crater stibnite
sulfate in Wakamiko Crater vent fluids
-40
-30
-20
-10
0
+10
+20
δ34SCDT (‰)

Figure 11